

## Application of Ionized Intrinsic Microporous Poly(phenyl-alkane)s as Alkaline Ionomers for Anion Exchange Membrane Water Electrolyzers<sup>1</sup>

Shu-Qing Fu,<sup>1</sup> Bin Hu,<sup>1</sup> Ji-Hong Ge, Ming-Zhi Zhu, Pan-Pan Huang, Boxin Xue,\* Nanwen Li,\*<sup>2</sup> and Pei-Nian Liu\*



Cite This: *Macromolecules* 2023, 56, 6037–6050 <sup>3</sup>



Read Online

ACCESS <sup>4</sup>

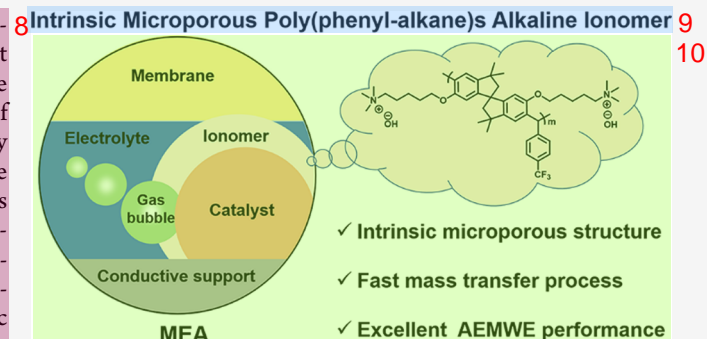
Metrics & More <sup>5</sup>

Article Recommendations <sup>6</sup>

Supporting Information <sup>7</sup>

**ABSTRACT:** Alkaline ionomers used in anion exchange membrane water electrolyzers (AEMWEs) require fast mass transport to maximize the activity of the catalytic reaction at the three-phase boundary. Taking advantage of the high free volume of polymers of intrinsic microporosity (PIMs), herein we propose a new strategy to apply ionized PIMs in the preparation of high-performance alkaline ionomers. A series of novel intrinsic microporous poly(phenyl-alkane) alkaline ionomers were synthesized by acid-catalyzed Friedel–Crafts polycondensation of electron-rich single-benzene/multi-benzene derivatives and trifluoromethyl/cyanide-substituted benzaldehydes. By adjusting the structure of aromatic monomers and aldehydes and the proportion of comonomers, the structures of the ionomer skeletons were systematically regulated.

By evaluating the microporosities, ion transport properties, and device properties, we found that introducing a twisted spirobisindane unit and a trifluoromethyl substituent to the poly(phenyl-alkane) skeleton promoted the formation of more micropore structures. Increased microporosity is beneficial for the construction of efficient and stable mass transfer channels, facilitating improved AEMWE performance ( $1685 \text{ mA cm}^{-2}$  at 1.8 V with a circulating 1 M NaOH solution at  $80^\circ\text{C}$ ) and excellent durability (>180 h at a high current density of  $1000 \text{ mA cm}^{-2}$ ). This work provides insights into the structure–property relationships of intrinsic microporous poly(phenyl-alkane) alkaline ionomers and demonstrates that ionic intrinsic microporous polymers are very promising candidates for the preparation of high-performance alkaline ionomers for AEMWEs.



- ✓ Intrinsic microporous structure
- ✓ Fast mass transfer process
- ✓ Excellent AEMWE performance

### 1. INTRODUCTION <sup>12</sup>

The production of green hydrogen ( $\text{H}_2$ ) via water electrolysis is attracting attention for its potential role and applicability in the large-scale utilization of renewable energy and decarbonization.<sup>1–4</sup> Among various water electrolysis technologies, the anion exchange membrane water electrolyzers (AEMWEs) combine the advantages of the low cost of alkaline water electrolyzers and the high efficiency of proton exchange membrane water electrolyzers.<sup>5–7</sup> Correspondingly, AEMWEs have shown great potential for commercialization.<sup>8</sup> The membrane electrode assembly (MEA) is the basic unit of an AEMWE and is mainly composed of an anion exchange membrane (AEM), a catalyst layer (CL), and a gas diffusion layer (GDL).<sup>3,9</sup> The structural design and components of MEAs directly determine the  $\text{H}_2$  output rate and cell efficiency of AEMWEs. Therefore, developing improved MEAs is crucial for the advancement of AEMWEs.<sup>10,11</sup> Alkaline ionomers are key components in MEAs, wherein they act as ionic conductive binders to create stable CLs between the AEM and GDL, establish efficient mass transfer channels in the CL, and reduce the contact resistance between the CL and AEM.<sup>3</sup> An ideal

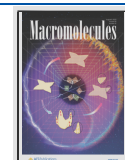
alkaline ionomer would enhance the utilization and stability of the catalyst, which are key to achieving high performance and long life of AEMWEs.<sup>12,13</sup>

However, the development of alkaline ionomers has been slow compared to that of AEMs, and the effect of alkaline ionomers on the performance of AEMWEs has been seriously underestimated.<sup>3</sup> Alkaline ionomers need to be specifically designed to have a positive impact on AEMWE performance. First, the ionomer needs to have fast conduction of ions, water molecules, and gas products to ensure an efficient catalytic reaction at the three-phase boundary. Second, the ionomer requires excellent overall stability, including chemical, thermal, and mechanical stabilities. Finally, the ionomer needs to have

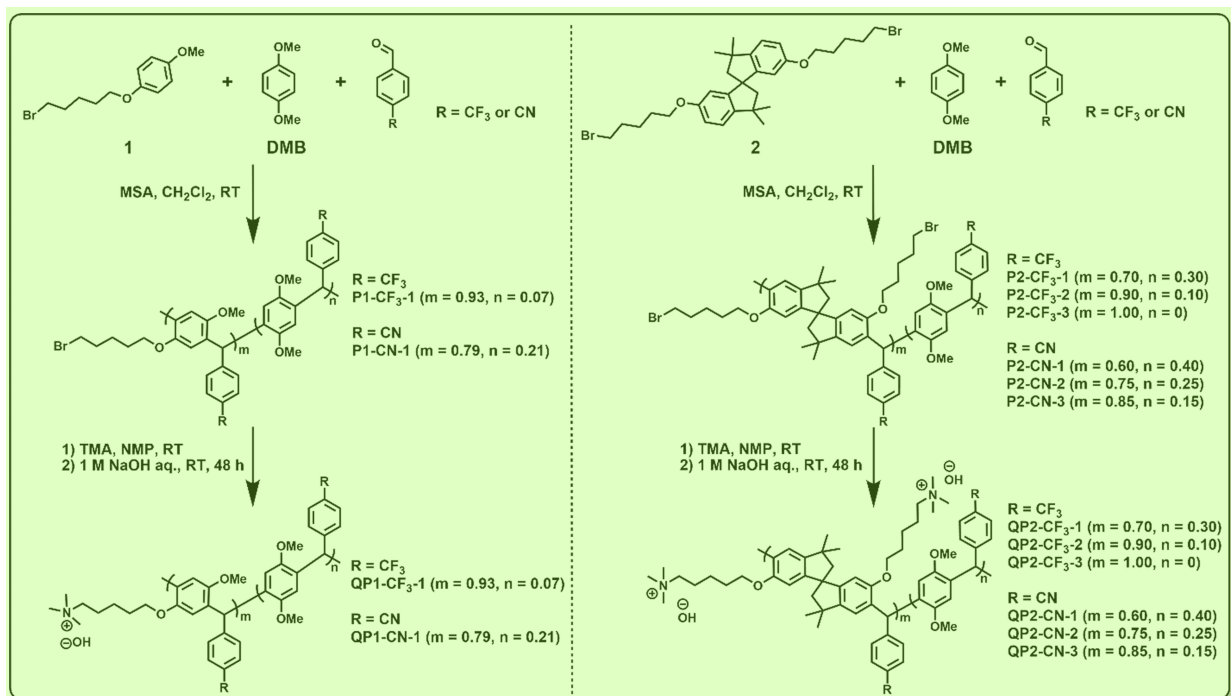
Received: April 18, 2023

Revised: July 4, 2023

Published: July 18, 2023



Scheme 1. Synthetic Route for Intrinsic Microporous Poly(phenyl-alkane) Alkaline Ionomers 1



good dispersion in low-boiling-point solvents and display excellent bonding ability with the catalyst.<sup>3</sup> The same polymer is often used in many studies to prepare both the ionomer and the AEM.<sup>14–19</sup> However, doing so disregards the different roles of the ionomer and AEM in electrolyzers. For example, AEMs need low gas permeability to suppress the crossover of oxygen ( $O_2$ ) and  $H_2$ . However, for the ionomers, low permeability will lead to the accumulation of gas product bubbles on the surface of the catalyst, which can trigger off a series of negative impacts (e.g., blocking active sites and hindering mass transfer) and ultimately reduce the catalytic reaction efficiency.<sup>3,12</sup> Therefore, using the exact same polymer system for AEM and the ionomer is not necessarily the best choice. On the premise of ensuring the fundamental properties (ion conductivity, chemical stability, thermal stability, etc.) of the ionomer, boosting the gas diffusion capacity is the urgent challenge to further improve the performance of AEMWEs.

Polymers of intrinsic microporosity (PIMs) constitute a family of amorphous porous polymers that have such advantageous properties as high free volume, solution processability, and good designability.<sup>20–23</sup> The structure of polymer chains can be easily regulated by designing the rigid and twisted molecular structure of polymerization monomers.<sup>24,25</sup> In recent years, ionized PIMs have been proposed for the preparation of highly conductive AEMs. For example, Yang et al. developed a PIM-based AEM with the rigid Tröger's base structures. The PIM-based AEM displayed high hydroxide conductivity, excellent dimensional stability, and good chemical stability.<sup>26</sup> Li et al. used a different approach and synthesized novel microporous AEMs that contained spirobisindane segments and cardo moieties. The AEM exhibited excellent hydroxide ion conductivity ( $165 \text{ mS cm}^{-1}$ ) at  $80^\circ\text{C}$ , which profited from the high free volume in the polymer facilitating the construction of well-developed hydroxide transportation channels.<sup>27</sup> Later, Wang et al. used the coplanar structure of 9,9-dimethylxanthrene to construct a

rigid and distorted inherent microporous skeleton, and the resulting AEM showed extremely high conductivity ( $205 \text{ mS cm}^{-1}$ ) and low swelling ratio (14.1%) at  $80^\circ\text{C}$ .<sup>28</sup> Although the microporous structure of PIMs is beneficial to construct effective ion transport channels and improve hydroxide conductivity, there are concerns that PIM-based AEMs may have high gas permeability due to the micropores. An increased AEM gas permeability could cause gas crossover between the electrodes, reduce  $H_2$  purity, and cause undetectable issues to the long-term safe operation of the cell. In contrast to AEMs, high gas permeability is one of the key characteristics required for alkaline ionomers,<sup>3,12</sup> and as such, we envision that ionized PIM skeletons may be well suited for alkaline ionomers.

In this study, we applied ionized PIMs to the development of high-performance alkaline ionomers for AEMWEs. First, we prepared the electron-rich single-benzene/multi-benzene derivatives (1 and 2), and 1,4-dimethoxybenzene (DMB) was chosen as the copolymerized aromatic monomer to polymerize with trifluoromethyl ( $CF_3$ )-/cyanide ( $CN$ )-substituted benzaldehydes by acid-catalyzed Friedel–Crafts polycondensation. Subsequently, quaternization of the poly(phenyl-alkane) precursors afforded eight alkaline ionomers (Scheme 1). By adjusting the structure of aromatic monomers and aldehydes, and the proportion of comonomers, the structures of the ionomer skeleton were easily regulated. By evaluating the microporous structures, ion transport properties, and device properties, the introduction of twisted spirobisindane units and trifluoromethyl groups to the poly(phenyl-alkane) skeleton was found to have several benefits. Specifically, the alterations lead to the increased formation of micropore structures, increased free volume, and facilitated the construction of efficient and stable mass transfer channels, hence obtaining excellent water electrolysis performance.

## 2. EXPERIMENTAL SECTION 1

**2.1. Materials.** 4-Methoxyphenol, 1,5-dibromopentane, potassium carbonate ( $K_2CO_3$ ), acetonitrile, petroleum ether (PE), dichloromethane (DCM), bisphenol A, methanesulfonic acid (MSA), ethanol (EtOH), 1,4-dimethoxybenzene (DMB), 4-cyanobenzaldehyde, 4-(trifluoromethyl)benzaldehyde, methanol (MeOH), trimethylamine (30% in ethanol) (TMA), *N*-methylpyrrolidone (NMP), ethyl acetate (EA), sodium chloride (NaCl), sodium hydroxide (NaOH), sodium nitrate ( $NaNO_3$ ), silver nitrate ( $AgNO_3$ ), potassium chromate ( $K_2CrO_4$ ), *N,N*-dimethylformamide (DMF), dimethyl sulfoxide (DMSO), and deuterium reagents [chloroform-*d* ( $CDCl_3\text{-}d$ ) and methanol-*d*<sub>4</sub> ( $CD_3OD\text{-}d_4$ )] were purchased and used as received. Deionized water (DI water, 18 MΩ) was degassed and used. 6,6'-Dihydroxy-3,3',3'-tetramethyl-1,1'-spirobisindane was synthesized according to the reported literature,<sup>29</sup> and the details are shown in Section S1 (Supporting Information).

**2.2. Monomer Synthesis.** 2.2.1. *Synthesis of 1-((5-Bromopentyl)oxy)-4-methoxybenzene (1).* The monomer was prepared referring to the reported literature studies.<sup>30,31</sup> 4-Methoxyphenol (6.5 mL, 80.6 mmol) and acetonitrile (100 mL) were added to a flask.  $K_2CO_3$  (22.3 g, 161.2 mmol) and 1,5-dibromopentane (22.0 mL, 161.2 mmol) were added under nitrogen ( $N_2$ ) flow conditions at 25 °C. The mixture was refluxed with stirring overnight, and then, it was filtered to get rid of  $K_2CO_3$  and concentrated by reducing pressure. The product was extracted by a short silica gel column eluting with PE:DCM (3:1), followed by concentration. Finally, monomer **1** was obtained as a colorless liquid (13.0 g, 59% yield). <sup>1</sup>H NMR (400 MHz,  $CDCl_3\text{-}d$ ):  $\delta$  6.84 (s, 4H), 3.92 (t,  $J$  = 6.3 Hz, 2H), 3.77 (s, 3H), 3.44 (t,  $J$  = 6.8 Hz, 2H), 1.93 (m, 2H), 1.79 (m, 2H), 1.62 (m, 2H); <sup>13</sup>C NMR (101 MHz,  $CDCl_3\text{-}d$ ):  $\delta$  153.80, 153.17, 115.44, 114.66, 68.22, 55.73, 33.73, 32.58, 28.60, 24.90; HRMS (EI, TOF): calc. for [M]: 272.0412, found for [M]: 272.0413.

2.2.2. *Synthesis of 6,6'-Bis((5-bromopentyl)oxy)-3,3,3',3'-tetramethyl-1,1'-spirobisindane (2).* 6,6'-Dihydroxy-3,3,3',3'-tetramethyl-1,1'-spirobisindane (5.0 g, 16.2 mmol) was added to a flask containing acetonitrile (100 mL).  $K_2CO_3$  (13.4 g, 97.3 mmol) and 1,5-dibromopentane (13.3 mL, 97.3 mmol) were added under  $N_2$  flow conditions at 25 °C. The mixture was refluxed with stirring overnight and then filtered to remove  $K_2CO_3$ , concentrated by rotary evaporation. The desired product was extracted via a short silica gel column eluting with PE:DCM (10:1), followed by concentration. Finally, monomer **2** was obtained as a white crystalline solid (4.0 g, 41% yield). <sup>1</sup>H NMR (400 MHz,  $CDCl_3\text{-}d$ ):  $\delta$  7.11 (d,  $J$  = 8.3 Hz, 2H), 6.81 (dd,  $J$  = 8.3, 2.3 Hz, 2H), 6.37 (d,  $J$  = 2.3 Hz, 2H), 3.89 (t,  $J$  = 6.3 Hz, 4H), 3.43 (t,  $J$  = 6.8 Hz, 4H), 2.38 (d,  $J$  = 13.0 Hz, 2H), 2.28 (d,  $J$  = 13.0 Hz, 2H), 1.93 (m, 4H), 1.77 (m, 4H), 1.61 (m, 4H), 1.42 (s, 6H), 1.36 (s, 6H); <sup>13</sup>C NMR (151 MHz,  $CDCl_3\text{-}d$ ):  $\delta$  158.79, 151.92, 144.69, 122.46, 113.72, 109.90, 67.71, 59.71, 57.87, 42.88, 33.67, 32.57, 31.88, 30.61, 28.59, 24.93; HRMS (EI, TOF): calc. for [M-CH<sub>3</sub>]: 591.1296, found for [M-CH<sub>3</sub>]: 591.1293; melting point: 110–112 °C.

**2.3. Polymer Synthesis.** 2.3.1. *Synthesis of P1-CF<sub>3</sub>-1.* The polymer was prepared referring to the reported literature studies.<sup>32–34</sup> A mixture of **1** (1.0 g, 3.66 mmol), 1,4-dimethoxybenzene (38.0 mg, 0.28 mmol), and 4-(trifluoromethyl)benzaldehyde (0.65 mL, 4.72 mmol) was dissolved in DCM (3.5 mL) in a 25 mL reaction flask. After 30 min, MSA (1.02 mL, 15.75 mmol) was dropped in the reaction mixture with constant stirring. The reaction continued for 24 h at 25 °C with the formation of a dark brown, gel-like mass, which showed a gradual increase in viscosity during the reaction time. The mass was diluted with 10.0 mL of DCM, and then the mixed solution was poured slowly into MeOH. A white fibrous solid was collected and further purified in MeOH by Soxhlet extraction for 24 h. After drying at 80 °C under vacuum overnight, 1.6 g of the white fibrous solid was gained (90% yield).

2.3.2. *Synthesis of P1-CN-1.* **1** (1.0 g, 3.66 mmol), 1,4-dimethoxybenzene (134.0 mg, 0.97 mmol), 4-cyanobenzaldehyde (729 mg, 5.56 mmol), and DCM (3.5 mL) were sequentially added into a round-bottomed flask (25 mL). After 30 min, MSA (1.20 mL,

18.54 mmol) was dropped in the reaction mixture with constant stirring. The polymerization proceeded for 28 h at 25 °C. During this time, a slow increase in the viscosity was observed until a dark-brown, gel-like mass was obtained. Then, 10.0 mL of DCM was used to dilute the mixture before slowly pouring it into MeOH. A white fibrous solid was collected and purified in MeOH by Soxhlet extraction for 24 h. After drying at 80 °C under vacuum overnight, the **P1-CN-1** copolymer (white fibrous solid, 1.6 g, 89% yield) was obtained.

2.3.3. *Synthesis of P2-CF<sub>3</sub>-1–3.* In the synthesis of **P2-CF<sub>3</sub>-1**, **2** (1.0 g, 1.65 mmol), 1,4-dimethoxybenzene (98.0 mg, 0.71 mmol), 4-(trifluoromethyl)benzaldehyde (0.39 mL, 2.83 mmol), and DCM (3.5 mL) were put into a round-bottomed flask (25 mL) successively. After 30 min, MSA (0.61 mL, 9.42 mmol) was dropped in the reaction mixture with constant stirring. The reaction continued for 16 h at 25 °C with the formation of a dark brown, gel-like mass, which showed a gradual increase in viscosity during the reaction time. Then, 10.0 mL of DCM was used to dilute the mixture before slowly pouring it into MeOH. A white fibrous solid was collected and purified in MeOH by Soxhlet extraction for 24 h. After drying at 80 °C under vacuum overnight, the **P2-CF<sub>3</sub>-1** copolymer (white fibrous solid, 1.3 g, 89% yield) was obtained.

**P2-CF<sub>3</sub>-2** and **P2-CF<sub>3</sub>-3** were obtained using the same procedure. For **P2-CF<sub>3</sub>-2**, the dosages of **2**, 1,4-dimethoxybenzene, 4-(trifluoromethyl)benzaldehyde, and MSA were 1 g (1.65 mmol), 25.3 mg (0.18 mmol), 0.30 mL (2.20 mmol), and 0.48 mL (7.33 mmol), respectively. For **P2-CF<sub>3</sub>-3**, the dosages of **2**, 1,4-dimethoxybenzene, 4-(trifluoromethyl)benzaldehyde, and MSA were 1 g (1.65 mmol), 0 mg, 0.27 mL (1.98 mmol), and 0.43 mL (6.60 mmol), respectively. The yields of **P2-CF<sub>3</sub>-2** (white fiber-like solid) and **P2-CF<sub>3</sub>-3** (white fiber-like solid) are 90 and 88%, respectively.

2.3.4. *Synthesis of P2-CN-1–3.* In the synthesis of **P2-CN-1**, **2** (1.0 g, 1.65 mmol), 1,4-dimethoxybenzene (151.9 mg, 1.10 mmol), 4-cyanobenzaldehyde (432.5 mg, 3.30 mmol), and DCM (3.5 mL) were put into a round-bottomed flask (25 mL) successively. After 30 min, MSA (0.71 mL, 10.99 mmol) was dropped in the reaction mixture with constant stirring. The reaction continued for 20 h at 25 °C with the formation of a dark brown, gel-like mass, which showed a gradual increase in viscosity during the reaction time. Then, 10.0 mL of DCM was used to dilute the mixture before slowly pouring it into MeOH. A white fibrous solid was collected and purified in MeOH by Soxhlet extraction for 24 h. After drying at 80 °C under vacuum overnight, the **P2-CN-1** copolymer (white fibrous solid, 1.3 g, 89% yield) was obtained.

**P2-CN-2** and **P2-CN-3** were obtained using the same procedure. For **P2-CN-2**, the dosages of **2**, 1,4-dimethoxybenzene, 4-cyanobenzaldehyde, and MSA were 1 g (1.65 mmol), 75.9 mg (0.55 mmol), 345.9 mg (2.64 mmol), and 0.57 mL (8.79 mmol), respectively. For **P2-CN-3**, the dosages of **2**, 1,4-dimethoxybenzene, 4-cyanobenzaldehyde, and MSA were 1 g (1.65 mmol), 40.2 mg (0.29 mmol), 305.2 mg (2.33 mmol), and 0.50 mL (7.76 mmol), respectively. The yields of **P2-CN-2** (white fiber-like solid) and **P2-CN-3** (white fiber-like solid) are 88 and 91%, respectively.

2.3.5. *Synthesis of Alkaline Ionomers QP1-CF<sub>3</sub>-1, QP1-CN-1, QP2-CF<sub>3</sub>-1–3, and QP2-CN-1–3.* Taking the synthesis of **QP2-CF<sub>3</sub>-1** as an example: TMA (30% in ethanol) was chosen as the quaternized reagent for the quaternization of **P2-CF<sub>3</sub>-1**, and the synthetic process of **QP2-CF<sub>3</sub>-1** is as follows: TMA (4.0 mL) was injected into the NMP (50 mL) solution of **P2-CF<sub>3</sub>-1** (1.0 g) at 25 °C. The reaction mixture was stirred for at least 48 h. Then, the solution was distilled to 15 mL and poured slowly into EA. The formed white fibrous solid was filtered and further washed 3 times with EA. The **QP2-CF<sub>3</sub>-1** ionomer (white solid, 90% yield) was obtained after drying at 80 °C under vacuum overnight.

**QP1-CF<sub>3</sub>-1**, **QP1-CN-1**, **QP2-CF<sub>3</sub>-2–3**, and **QP2-CN-1–3** were prepared using the same procedure. These products are all white fibrous solids in nature. The yields of **QP1-CF<sub>3</sub>-1**, **QP1-CN-1**, **QP2-CF<sub>3</sub>-2**, **QP2-CF<sub>3</sub>-3**, **QP2-CN-1**, **QP2-CN-2**, and **QP2-CN-3** are 90, 89, 91, 88, 90, and 89%, respectively.

2.4. *Preparation of Membranes.* To prepare the membranes, an NMP solution (2–4 wt %) of the quaternized polymer (0.3 g in

bromide anion ( $\text{Br}^-$ ) form) was prepared and then poured onto a clean glass plate ( $0.1 \text{ m} \times 0.1 \text{ m}$ ) at  $80^\circ\text{C}$  for 5 h. Finally, the membrane was peeled off by soaking the glass plate in DI water.

**2.4.1. Ion Exchange of Membranes to Chloride Anion Form.** The membrane in  $\text{Br}^-$  form was soaked in a  $\text{NaCl}$  aqueous solution (1 M) for 48 h at  $25^\circ\text{C}$ . The membrane in chloride anion ( $\text{Cl}^-$ ) form was fully washed with DI water to get rid of the residual  $\text{NaCl}$ . Prior to testing, the  $\text{Cl}^-$ -type membrane was reserved in DI water.

**2.4.2. Ion Exchange of Membranes to Hydroxide Anion Form.** The membrane in  $\text{Br}^-$  form was soaked in a  $\text{NaOH}$  aqueous solution (1 M) for 48 h at  $25^\circ\text{C}$  to replace  $\text{Br}^-$  with hydroxide anion ( $\text{OH}^-$ ). Then, the  $\text{OH}^-$ -type membrane was fully washed with degassed DI water until the pH of the aqueous solution became neutral. Prior to testing, the membrane in  $\text{OH}^-$  form was stored in degassed DI water.

**2.5. Characterization.** In Section S2 of the Supporting Information, a detailed description of molecular structure analysis and microstructure characterization is provided through the analysis of various spectra including proton nuclear magnetic resonance ( $^1\text{H}$  NMR), carbon-13 nuclear magnetic resonance ( $^{13}\text{C}$  NMR), high-resolution mass spectrometry (HRMS), Fourier transform infrared spectroscopy (FTIR), gel permeation chromatography, atomic force microscopy (AFM), and small-angle X-ray scattering (SAXS). In addition, property characterizations of alkaline ionomers including inherent viscosity ( $\eta$ ), ion exchange capacity (IEC), microporosity, density ( $\rho$ ), fractional free volume (FFV), gas permeability, water uptake (WU), swelling ratio (SR), ion conductivity ( $\sigma$ ), mechanical property, thermal stability, chemical stability, water electrolysis performance, electrochemical impedance spectroscopy (EIS), cyclic voltammetry (CV), electrochemical surface area (ECSA), and linear sweep voltammetry (LSV) are presented in Section S3 of the Supporting Information.

### 3. RESULTS AND DISCUSSION<sup>4</sup>

**3.1. Monomer and Polymer Synthesis.** It has been demonstrated that acid-catalyzed Friedel–Crafts polycondensation of electron-rich single-benzene/multi-benzene derivatives and benzaldehydes with electron-withdrawing substituents is an effective method for the synthesis of high-molecular-weight poly(phenyl-alkane)s.<sup>32–36</sup> Previously, the incorporation of ionic functional groups in AEMs or ionomers usually involved harsh, multi-step, or uncontrollable modifications of aldehydes,<sup>32,35</sup> with such methods being undesirable. In the present study, we designed two novel aromatic monomers adorned with a suspended haloalkyl side chain: a 1,4-disubstituted single-benzene derivative **1** and a multi-benzene derivative containing the rigid and twisted spirobisindane structure **2**. Monomers **1** and **2** were prepared by regular nucleophilic substitution reactions of phenol derivatives (Scheme S1). The chemical structures of **1** and **2** were confirmed by  $^1\text{H}$  NMR,  $^{13}\text{C}$  NMR, and mass spectroscopy, respectively (Figures S1–S7, Supporting Information).

The next step was the synthesis of the relevant polymers through Friedel–Crafts polycondensation. In addition to the prepared **1** and **2**, 1,4-dimethoxybenzene (DMB) was selected as an aromatic comonomer to adjust the IEC of the ionomers. Furthermore, two benzaldehydes with electron-withdrawing substituents (*p*-trifluorobenzaldehyde and *p*-cyanobenzaldehyde) were chosen to polymerize with these aromatic monomers. All the Friedel–Crafts polycondensation reactions were performed in MSA and DCM at room temperature under vigorous stirring. During Friedel–Crafts polycondensation, the Gibbs activation energy of the first step is higher than that of the second, which allows nonstoichiometric polycondensations and a dramatic increase in the molecular weight of the polymers.<sup>37,38</sup> In this polymerization system, the amounts of aldehydes are 1.2 times the total amount of aromatic

monomers. Notably, the polymerization stopping time is important as extended reaction times would result in insoluble polymer formation. As such, once the mixture in the polymerization system formed an elastic ball, excess DCM needs to be added into the reaction system to terminate the polymerization. The structure of the polymer backbone was easily tuned by using different monomer combinations and varying the ratio of aromatic monomers (**1** or **2**/DMB). Eight analogues of poly(phenyl-alkane) precursor polymers (**P1-CF<sub>3</sub>-1**, **P1-CN-1**, **P2-CF<sub>3</sub>-1–3**, and **P2-CN-1–3**) were successfully prepared. The polymerization reaction time and molecular weight information are shown in Table 1. The

**Table 1. Polymerization Reaction Time and Molecular Weight Properties of Precursor Polymers**

polymer	time (h)	$M_n$ <sup>a</sup> ( $\times 10^4$ Da)	$M_w$ <sup>b</sup> ( $\times 10^4$ Da)	PDI <sup>c</sup>
<b>P1-CF<sub>3</sub>-1</b>	24	23.1	61.7	2.67
<b>P2-CF<sub>3</sub>-1</b>	16	19.7	41.4	2.10
<b>P2-CF<sub>3</sub>-2</b>	20	17.0	37.4	2.20
<b>P2-CF<sub>3</sub>-3</b>	16	10.4	30.5	2.92
<b>P1-CN-1</b>	28	10.2	62.1	6.11
<b>P2-CN-1</b>	20	83.3	94.5	1.13
<b>P2-CN-2</b>	18	91.6	100.0	1.09
<b>P2-CN-3</b>	20	119.5	136.1	1.14

<sup>a</sup>Number-average molecular weight ( $M_n$ ). <sup>b</sup>Weight-average molecular weight ( $M_w$ ). <sup>c</sup>PDI =  $M_w/M_n$ .

number-average molecular weights ( $M_n$ ) of the poly(phenyl-alkane) precursor polymers range from  $10.2 \times 10^4$  to  $119.5 \times 10^4$  Da, indicating that Friedel–Crafts polycondensation proceeded efficiently.

Finally, the targeted alkaline ionomers, **QP1-CF<sub>3</sub>-1**, **QP1-CN-1**, **QP2-CF<sub>3</sub>-1–3**, and **QP2-CN-1–3**, were prepared by the Menshutkin reaction of the precursor polymers with trimethylamine. The inherent viscosity of these alkaline ionomers ranges from 0.36 to 0.66 dL g<sup>-1</sup> (Table S1), showing good consistence with the molecular weight of the corresponding precursor polymers. The solubilities of the alkaline ionomers as well as their precursor polymers are summarized in Table S2. Notably, these alkaline ionomers not only can be dissolved in *N*-methylpyrrolidone, *N,N*-dimethylformamide, and dimethyl sulfoxide but also show good solubility in alcohol solvents such as methanol. These desirable solubility profiles enabled their application as ionomer materials in MEAs.

The chemical structures of all the precursor polymers and alkaline ionomers were characterized with  $^1\text{H}$  NMR and FTIR spectroscopy (Figures S8–S12). The representative  $^1\text{H}$  NMR spectra of the precursor polymer series (**P1-CF<sub>3</sub>-1**, **P1-CN-1**, **P2-CF<sub>3</sub>-1**, and **P2-CN-1**) are shown in Figure 1. The chemical shifts at approximately 7.42–7.57 ppm and 7.10–7.23 ppm in the spectra of **P1-CF<sub>3</sub>-1** and **P1-CN-1** were assigned to aromatic protons on the aldehyde residue, while the signals at approximately 5.99–6.18 ppm were assigned to methine of the triphenylmethane moiety. Finally, the signals at 3.14–3.28 ppm and 3.35–3.48 ppm were attributed to  $-\text{CH}_2\text{Br}$  in the bromopentyl group and methoxy groups from **1** and DMB, respectively. Owing to their structural similarity to **P1-CF<sub>3</sub>-1** and **P1-CN-1**, the  $^1\text{H}$  NMR spectra of **P2-CF<sub>3</sub>-1** and **P2-CN-1** contained similar signals assigned to the aldehyde, triphenylmethane, methoxy, and  $-\text{CH}_2\text{Br}$  protons. One obvious difference between the **P1** and **P2** polymer precursors is the

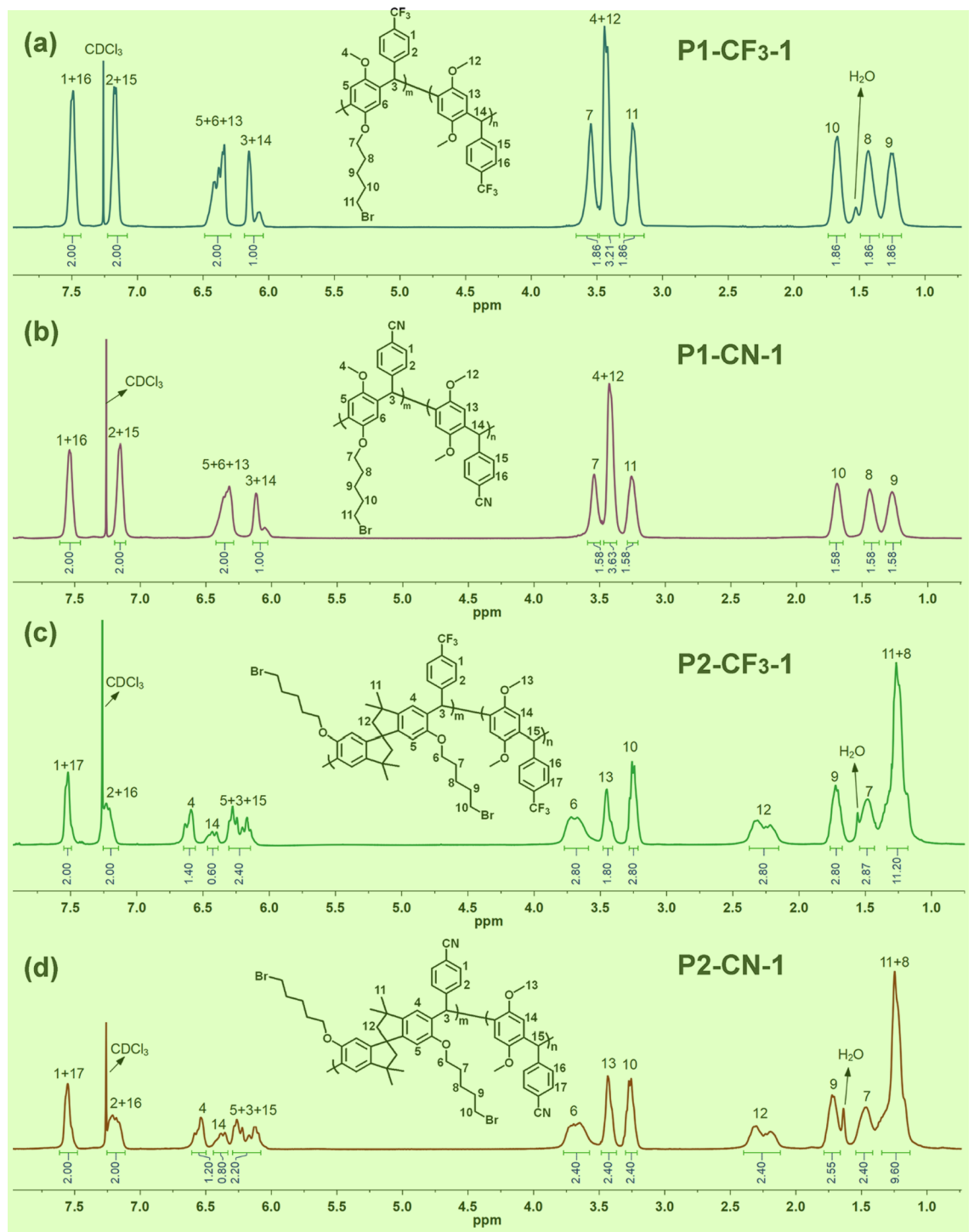


**Figure 1.**  $^1\text{H}$  NMR spectra of (a) P1-CF<sub>3</sub>-1, (b) P1-CN-1, (C) P2-CF<sub>3</sub>-1, and (d) P2-CN-1.<sup>2</sup>

proton signals assigned to the spirobisindane methylene groups<sup>3</sup> that appear at 2.10–2.40 ppm. The  $^1\text{H}$  NMR analysis of all precursor polymers indicated that the ratio of the two different repeating units ( $m$  and  $n$  in Scheme 1) matched well with the monomer feed ratio (1 or 2/DMB) used during polymerization (Figures S8 and S9). The  $^1\text{H}$  NMR spectra of the ionomers are shown in Figures S10 and S11, and new signals were observed at approximately 3.09 ppm and were assigned to the protons of methyl groups from the trimethylpentyl ammonium moiety. In addition, the FTIR spectra of the ionomers contained bands at 1650  $\text{cm}^{-1}$ , which were assigned

to the stretching vibrations of  $-\text{N}(\text{CH}_3)^+$  (Figure S12). These<sup>4</sup> results indicate that the quaternization reaction proceeded smoothly.

**3.2. Membrane Preparation and Ion Exchange Capacity.** The alkaline ionomers can be cast into flexible and transparent membranes from 2–4 wt % NMP solutions (Figure S13). After soaking in aqueous NaCl and NaOH solutions, membranes in chloride anion ( $\text{Cl}^-$ ) and hydroxide anion ( $\text{OH}^-$ ) forms can be obtained, respectively. The IEC values for the alkaline ionomers were calculated based on the known monomer feed ratios and experimentally measured

**Table 2.** Properties of Alkaline Ionomers 1

sample	IEC (mmol g <sup>-1</sup> )	IEC <sub>theo</sub> <sup>a</sup>	IEC <sub>titr</sub> <sup>b</sup>	S <sub>BET</sub> <sup>c</sup> (m <sup>2</sup> g <sup>-1</sup> )	WU <sup>d</sup> (%)	SR <sup>d</sup> (%)	σ (Cl <sup>-</sup> ) <sup>e</sup> (mS cm <sup>-1</sup> )	σ (OH <sup>-</sup> ) <sup>f</sup> (mS cm <sup>-1</sup> )	q <sup>g</sup> (nm <sup>-1</sup> )	d <sup>g</sup> (nm)
QP1-CF <sub>3</sub> -1	2.23	2.21		35.5	36	26	50.4	77.8	2.12	2.96
QP2-CF <sub>3</sub> -1	2.27	2.25		59.2	40	28	68.5	113.3	2.21	2.84
QP2-CF <sub>3</sub> -2	2.54	2.50		65.0	86	50	71.7	140.3	2.27	2.77
QP2-CF <sub>3</sub> -3	2.65	2.62		69.0	124	70	90.7	144.4	2.30	2.73
QP1-CN-1	2.23	2.20		31.3	1	10	41.1	67.1	2.02	3.11
QP2-CN-1	2.27	2.23		35.3	5	15	58.8	93.7	2.25	2.79
QP2-CN-2	2.51	2.48		47.8	81	33	68.6	124.7	2.28	2.75
QP2-CN-3	2.64	2.60		54.2	96	70	73.9	141.9	2.32	2.71

<sup>a</sup>Theoretical value, calculated from the ratio of complete conversion. <sup>b</sup>Experimental value measured by titration. <sup>c</sup>BET single point surface area at  $P/P_0 = 0.03$ . <sup>d</sup>Measured in a OH<sup>-</sup> form membrane at the temperature of 30 °C under fully hydrated conditions (immersed). <sup>e</sup>Cl<sup>-</sup> conductivity, measured in a Cl<sup>-</sup> form membrane at the temperature of 80 °C under fully hydrated conditions (immersed). <sup>f</sup>OH<sup>-</sup> conductivity, measured in a OH<sup>-</sup> form membrane at the temperature of 80 °C under fully hydrated conditions (immersed). <sup>g</sup>Measured by SAXS in Cl<sup>-</sup> form in the dry state.

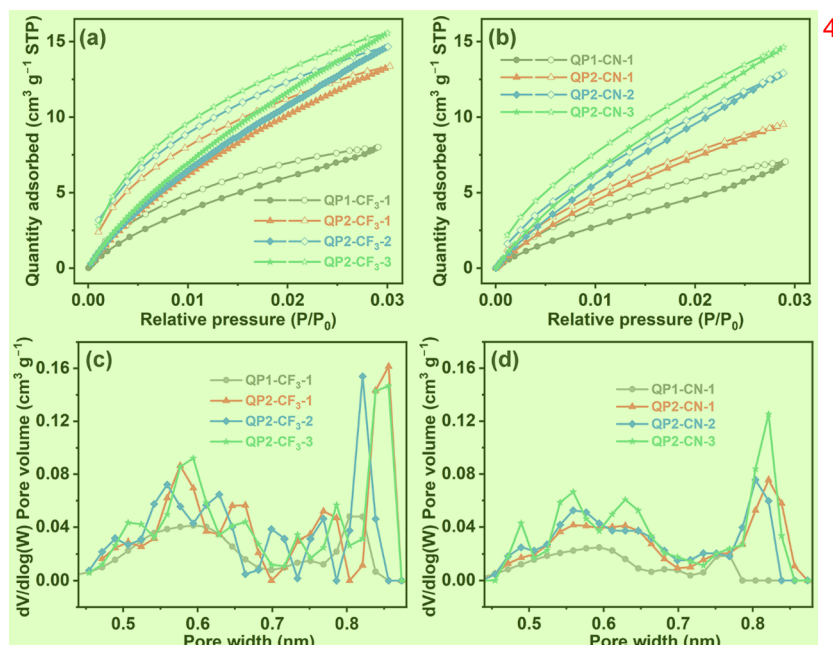


**Figure 2.** CO<sub>2</sub> adsorption–desorption isotherms at 273 K of (a) QP1-CF<sub>3</sub>-1 and QP2-CF<sub>3</sub>-1-3, and (b) QP1-CN-1 and QP2-CN-1-3 (The 5 adsorption branches are labeled with filled symbols, and the desorption branches are labeled with empty symbols). Pore size distributions of (c) QP1-CF<sub>3</sub>-1 and QP2-CF<sub>3</sub>-1-3, and (d) QP1-CN-1 and QP2-CN-1-3 from CO<sub>2</sub> sorption isotherms at 273 K based on NLDFT calculation.

through titration (Table 2). It was observed that the calculated values were similar to the experimental values. Furthermore, it can be seen from the experimental and calculated values that the IEC is regulated by the monomer ratio of the polymers. For example, for QP2-CF<sub>3</sub>-1-3 and QP2-CN-1-3, their IECs gradually increased with the increasing amounts of spirobisisindane monomer 2. As such, the IECs and structures of the alkaline ionomers can be easily regulated by adjusting the feed ratio of the polymerization monomers. Therefore, ionomer synthesis enabled us to undertake a systematic study of structure–property relationships.

**3.3. Intrinsic Microporous Structure, Fractional Free 7 Volume, and Gas Permeability.** To evaluate the intrinsic microporous structures of the alkaline ionomers, gas adsorption analyses were conducted at 273 K with carbon dioxide (CO<sub>2</sub>) as the probe. We divided the eight alkaline ionomers into two categories, CF<sub>3</sub>-substituted series (QP1-CF<sub>3</sub>-1, QP2-CF<sub>3</sub>-1, QP2-CF<sub>3</sub>-2, and QP2-CF<sub>3</sub>-3) and CN-substituted series (QP1-CN-1, QP2-CN-1, QP2-CN-2, and

QP2-CN-3). Each of the series can be further subdivided into 8 ionomers with or without the spirobisisindane structure.

The CO<sub>2</sub> adsorption–desorption isotherms of the CF<sub>3</sub>-substituted series and CN-substituted series are shown in Figure 2a,b, respectively. Comparatively, QP1-CF<sub>3</sub>-1 and QP2-CF<sub>3</sub>-1 have similar IEC values, while the spirobisisindane containing QP2-CF<sub>3</sub>-1 has a higher surface area (Table 2). Additionally, it can be observed that the surface area increases with increasing spirobisisindane content (QP2-CF<sub>3</sub>-1, QP2-CF<sub>3</sub>-2, and QP2-CF<sub>3</sub>-3). The same correlations can be drawn by analyzing the data of the CN-substituted ionomers. These results indicate that the rigid and twisted spirobisisindane structures are beneficial to inhibit chain stacking of the polymer chains and induce the formation of microporous structures.

On comparison of ionomers with a similar skeleton structure and consistent IECs, it was observed that the CF<sub>3</sub>-substituted ionomers have higher surface areas than the corresponding CN-substituted ionomers (Table 2). We propose two possible explanations for these phenomena: (1) the presence of –CF<sub>3</sub>

groups may increase the rotation rigidity of the backbones, limit the conformational freedom of the polymer backbones, and create more micropores; (2) the presence of polar  $-\text{CN}$  groups may enhance the intra/intermolecular interactions of the polymer backbone,<sup>39</sup> therefore leading to tighter packing of the polymer chains and decreased free volume.

The pore size distribution profiles were calculated using nonlocal density functional theory (NLDFT) (Figure 2c,d). The calculations reveal the existence of subnanometer-sized pores in the alkaline ionomers, further affirming the intrinsic microporosity of the ionomers. In conclusion, the above results indicate that the microporous structure of the ionomers can be tuned by the monomer structure and ratio. As such, these ionomers offer a platform to study the relationships between microporosity and property at a molecular level.

The FFV brought by the intrinsic microporous structure was evaluated by measuring the density of the dry membranes. As shown in Table S3, the free volume values of the ionomer range from 0.05 to 0.124 and increase with the introduction of a spirobisdindane structure, which are in good agreement with the BET values. Then, the  $\text{H}_2$  and  $\text{O}_2$  permeability of these ionomers in  $\text{Br}^-$  form was explored. As shown in Figure 3,  $\text{H}_2$

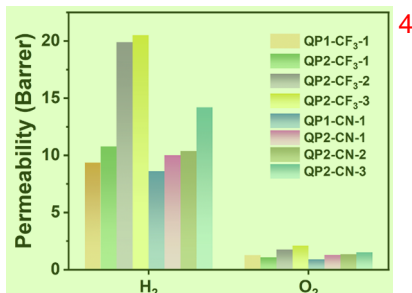


**Figure 3.** Gas permeance of the resulting alkaline ionomers in  $\text{Br}^-$  form at 35 °C under the dry state.

and  $\text{O}_2$  permeability increases with increasing spirobisdindane content. In addition, the  $\text{CF}_3$ -substituted ionomers generally exhibit higher permeability. Among them, QP2-CF<sub>3</sub>-3 exhibits the highest permeability, with a  $\text{H}_2$  permeability of 20.5 barrier and an  $\text{O}_2$  permeability of 2.1 barrier. In summary, these results further confirmed that these polymers are permeable ionomers.

#### 3.4. Water Uptake, Swelling Ratio, and Conductivity.

The existence of enough water molecules in the ionomer not only is conducive to ion dissociation but also facilitates the rapid migration of ions in the percolating water-rich phase domain.<sup>40</sup> Generally, the WU and SR are directly related to the IEC values, but there are outliers. As shown in Figure S14a,b, in the  $\text{CF}_3$ -substituted series, spirobisdindane-containing ionomers display higher WU and SR, particularly at high temperatures. We hypothesize that this is due to a higher free volume enabling higher water adsorption. Additionally, as the IEC and spirobisdindane content increase, the WU and SR values increase. The CN-substituted ionomers display the same correlations (Figure S14c,d). Furthermore, the  $\text{CF}_3$ -substituted ionomers have higher WU and SR values than the corresponding CN-substituted counterparts. Alongside the reduced free volume in the CN-substituted ionomers, we hypothesize that the introduction of the polar CN groups to the polymer skeleton strengthens intra/intermolecular interactions and therefore decreases the WU and SR.

High ion conduction is vital to increasing the mass transfer process of the CL. EIS was performed to test the  $\text{Cl}^-$  and  $\text{OH}^-$  conductivity of the ionomers. Nyquist plots of the ionomers in  $\text{Cl}^-$  and  $\text{OH}^-$  forms measured at different temperatures in the fully hydrated state showed the temperature dependence of ion conductivities (Figures S15 and S16). The  $\text{Cl}^-$  and  $\text{OH}^-$  conductivities of the  $\text{CF}_3$ -substituted series are shown in Figure 4a,b. The  $\text{Cl}^-$  conductivity of QP2-CF<sub>3</sub>-3, the ionomer with the highest IEC, reaches 90.7 mS cm<sup>-1</sup> at 80 °C. This is a particularly high level of  $\text{Cl}^-$  conduction and compares favorably to many literature-reported values.<sup>41–45</sup> In addition,

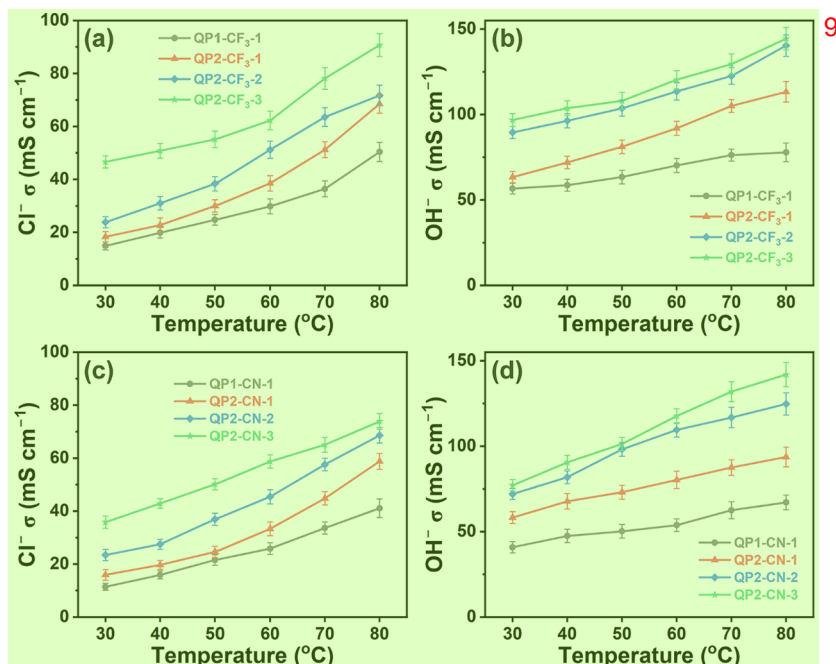


**Figure 4.** Temperature dependence of (a)  $\text{Cl}^-$  and (b)  $\text{OH}^-$  conductivities of QP1-CF<sub>3</sub>-1 and QP2-CF<sub>3</sub>-1–3. The temperature dependence of (c)  $\text{Cl}^-$  and (d)  $\text{OH}^-$  conductivities of QP1-CN-1 and QP2-CN-1–3.

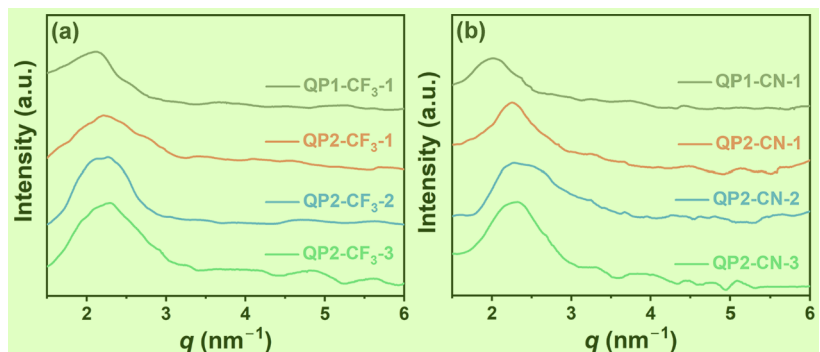


**Figure 5.** SAXS profiles of (a) QP1-CF<sub>3</sub>-1 and QP2-CF<sub>3</sub>-1–3 and (b) QP1-CN-1 and QP2-CN-1–3. **2**

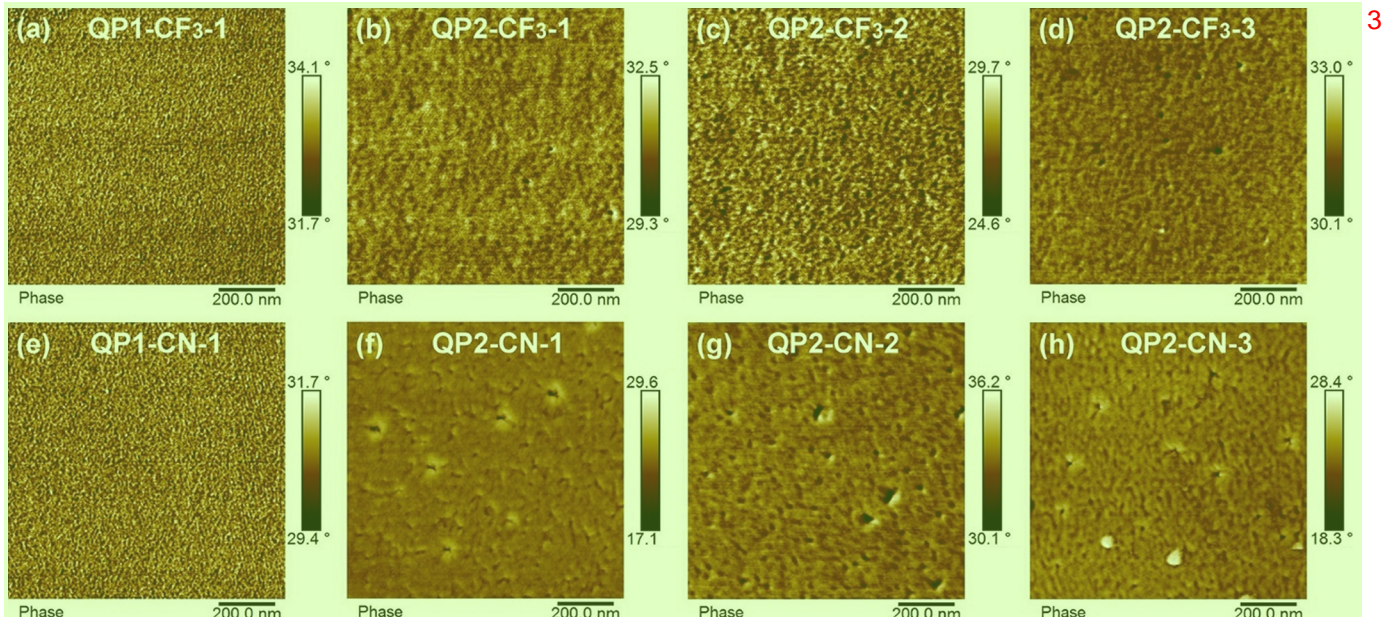


**Figure 6.** Microphase separation structure of the prepared ionomers in the Cl<sup>-</sup> form. AFM phase images of (a) QP1-CF<sub>3</sub>-1, (b) QP2-CF<sub>3</sub>-1, (c) QP2-CF<sub>3</sub>-2, (d) QP2-CF<sub>3</sub>-3, (e) QP1-CN-1, (f) QP2-CN-1, (g) QP2-CN-2, and (h) QP2-CN-3. **4**

its OH<sup>-</sup> conductivity was 144.4 mS cm<sup>-1</sup> at 80 °C, despite the influence of CO<sub>2</sub> not being excluded. The Cl<sup>-</sup> and OH<sup>-</sup> conductivities of the CN-substituted series are shown in Figure 4c,d. With a similar ionic content, the conductivity of the CN-substituted series was significantly lower than that of the CF<sub>3</sub>-substituted series. In addition, although QP1-CF<sub>3</sub>-1, QP2-CF<sub>3</sub>-1, QP1-CN-1, and QP2-CN-1 have similar IEC values (2.23–2.27 mmol g<sup>-1</sup>), QP2-CF<sub>3</sub>-1 and QP2-CN-1 show much higher OH<sup>-</sup> and Cl<sup>-</sup> conductivities. We postulate that this is because of the introduction of the spirobisindane unit. In summary, these results are consistent with the sequence of WU and specific area values, further proving that the microporous structure serves as an efficient channel for water and ion transport in the ionomers. **5**

**3.5. Microstructure.** The SAXS diagrams of the ionomers were measured (Figure 5), and the clear ionomer peak reveals the presence of a microphase separation structure within the ionomers. The characteristic separation length (*d*) can be calculated from the equation of  $d = 2\pi/q_{\max}$  (where  $q_{\max}$  is the maximum scattering vector). <sup>35,40</sup> The corresponding *d* of QP1-CF<sub>3</sub>-1, QP2-CF<sub>3</sub>-1, QP2-CF<sub>3</sub>-2, QP2-CF<sub>3</sub>-3, QP1-CN-1, QP2-CN-1, QP2-CN-2, and QP2-CN-3 is 2.96, 2.84, 2.77, 2.73, 3.12, 2.79, 2.75, and 2.71 nm, respectively (Table 2). Notably, the characteristic separation length of the ionomers **6**

does not have a strong correlation with the corresponding IEC. **7** The scattering peak shift can be ascribed to the aggregation behavior of the ion-containing side chains. <sup>46</sup> The structure and IEC of the ionomers both had a large influence on the SAXS profile and hence on the formation of ionic clusters. <sup>47</sup> Structurally, the rigid and twisted skeleton can promote the formation of more micropores within the QP2 membranes. We suppose that these micropores may impede the efficient aggregation of ion-containing segments and thus prevent the formation of large clusters even at high IECs. **8**

Direct observation of the morphologies of the ionomers was conducted by AFM. As shown in Figure 6, the phase separation is not prominent in QP1-CF<sub>3</sub>-1 and QP1-CN-1. However, a microphase separation morphology can be observed in QP2-CF<sub>3</sub>-1–3 and QP2-CN-1–3, in which the dark area represents the hydrophilic regions, and the bright area represents the hydrophobic regions. <sup>48–50</sup> More distinct microphase separation can be observed with increasing amounts of the spirobisindane monomer in the polymer backbone. It may be due to the fact that the increased hydrophilicity and flexibility of the cation enhance the difference between the hydrophilic and hydrophobic segments, hence facilitating the formation of ion clusters in the ionomers. <sup>51–53</sup> **9**

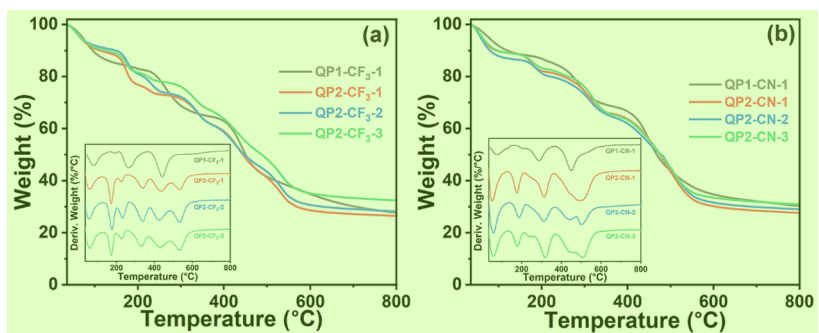


**Figure 7.** TGA curves of (a) QP1-CF<sub>3</sub>-1 and QP2-CF<sub>3</sub>-1–3 and (b) QP1-CN-1 and QP2-CN-1–3 under a N<sub>2</sub> atmosphere with a heating rate of 10 °C min<sup>-1</sup> [inset: DTG curves of (a) QP1-CF<sub>3</sub>-1 and QP2-CF<sub>3</sub>-1–3 and (b) QP1-CN-1 and QP2-CN-1–3].

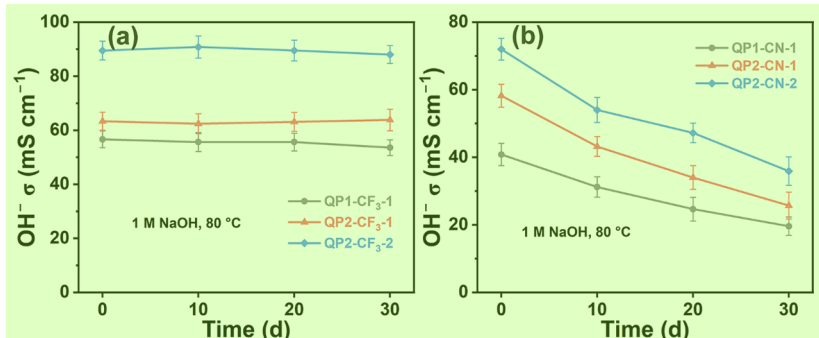


**Figure 8.** OH<sup>−</sup> conductivity changes of (a) QP1-CF<sub>3</sub>-1, QP2-CF<sub>3</sub>-1, and QP2-CF<sub>3</sub>-2 and (b) QP1-CN-1, QP2-CN-1, and QP2-CN-2 in a 1 M NaOH solution at 80 °C for 30 days.

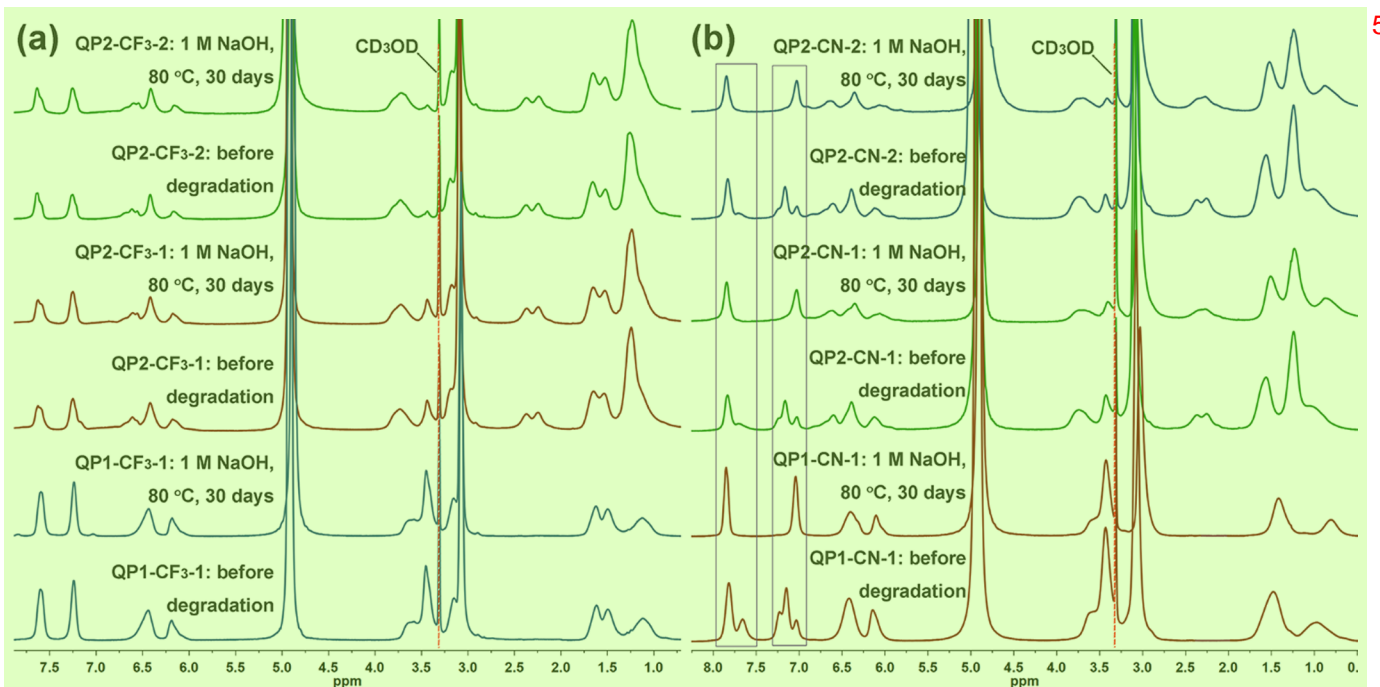


**Figure 9.** <sup>1</sup>H NMR changes of (a) QP1-CF<sub>3</sub>-1, QP2-CF<sub>3</sub>-1, and QP2-CF<sub>3</sub>-2 and (b) QP1-CN-1, QP2-CN-1, and QP2-CN-2 after immersion in a 1 M NaOH solution at 80 °C for 30 days.

**3.6. Mechanical Property, Thermal Stability, and Alkaline Stability.** Excellent mechanical properties of ionomers are essential for building robust MEAs. As such, we assessed the mechanical properties of the synthesized ionomers. The stress–strain curves of the ionomers are shown in Figure S17. The tensile strength and the elongation at break increase after incorporation of the spirobisindane monomer.

QP1-CF<sub>3</sub>-1 and QP1-CN-1 displayed the poorest mechanical properties. We postulate that this may be attributed to the presence of short rigid repeating units that inhibit chain entanglement of the polymers and weaken the interaction between polymer chains.<sup>35</sup> While assessing the properties of QP2-CF<sub>3</sub>-1–3 and QP2-CN-1–3, it became clear that the tensile strength decreased and the elongation at break

increased with the increasing content of spirobisindane monomer. This phenomenon can be explained as follows: ionomers with a higher IEC will absorb more water from the air, which acts as a plasticizer and leads to lower tensile strength;<sup>54,55</sup> simultaneously, the spirobisindane structure may enhance the toughness of the polymer chains.

To evaluate the thermal stability of the prepared ionomers, thermogravimetric analysis (TGA) and derivative thermogravimetry (DTG) curves were obtained, as shown in Figure 7. For QP1-CF<sub>3</sub>-1 and QP1-CN-1, the first weight loss between 50 and 200 °C was derived from the evaporation of the residual water and solvent within the ionomers. In the temperature range of 200–370 °C, the weight loss can be attributed to the degradation of the cations and side chains. The final stage (>370 °C) involved the decomposition of the polymer backbone. Comparatively, QP2-CF<sub>3</sub>-1–3 and QP2-CN-1–3 appear to have a more complicated weight loss process, likely owing to their more complex structures. However, QP2-CF<sub>3</sub>-1–3 and QP2-CN-1–3 underwent generally similar major degradation processes. Therefore, these results indicate that the prepared ionomers possess the requisite thermal stability for the application as binder materials.

The chemical stability of the AEMs and ionomers under harsh alkaline conditions is an important topic of current research. Their stability is mainly determined by the structure of the polymer backbone, side chain, and cationic head groups.<sup>40,56</sup> The alkaline stability of the prepared ionomers was first evaluated by monitoring the changes of OH<sup>−</sup> conductivity during the treatment in a 1 M NaOH solution at 80 °C. For the CF<sub>3</sub>-substituted series, the OH<sup>−</sup> conductivity remained stable throughout the alkaline stability test (Figure 8a), indicative of excellent chemical stability. However, for the CN-substituted series, the OH<sup>−</sup> conductivity decreased significantly with extended exposure to alkaline conditions (Figure 8b), possibly due to alkaline hydrolysis of the CN groups.<sup>57,58</sup> Alkaline hydrolysis of the CN groups would lead to carboxyl formation, and these groups have a strong electrostatic interaction with quaternary ammonium, which may explain the loss of OH<sup>−</sup> conductivity.

Changes to the chemical structure of the ionomers before and after the alkaline treatment were assessed to further study their alkaline stability. The <sup>1</sup>H NMR and FTIR spectra of the ionomers before and after the alkaline resistance test in a 1 M NaOH solution at 80 °C for 30 days are shown in Figures 9 and 10, respectively. For the CF<sub>3</sub>-substituted ionomers, no changes in chemical shift were observed in the <sup>1</sup>H NMR spectra (Figure 9a). Meanwhile, in the FTIR spectra (Figure 10a), there were no changes to peak intensity nor any new

peaks, even after 30 days in the 1 M NaOH solution at 80 °C.<sup>7</sup> This result is consistent with the conductivity test above and indicative of high chemical stability.

For CN-substituted ionomers, changes to the signals at 7.57–7.97 ppm and 6.87–7.37 ppm in the <sup>1</sup>H NMR spectra (Figure 9b) were observed. While a new band was observed at 1544 cm<sup>−1</sup> (−COONa), and the characteristic band of −CN at 2226 cm<sup>−1</sup> was no longer present in the FTIR spectra (Figure 10b). These observations are indicative of significant changes to the polymer structure and poor chemical stability. In a hot NaOH solution, the −CN groups are susceptible to attack by OH<sup>−</sup>, forming carboxylates and causing a change to the chemical environment of the aromatic protons on the aldehyde residue. Comparatively, the presence of inert −CF<sub>3</sub> groups in the polymer backbone may preclude hydrophilic OH<sup>−</sup> from attacking the polymer backbone, making the CF<sub>3</sub>-substituted ionomers more chemically stable. In addition, it is worth noting that except for the local changes in the aromatic region caused by −CN groups, other structures on the skeleton are still well preserved, indicating that the alkyl side chains and quaternary ammonium groups are chemically stable under alkaline conditions.

### 3.7. Impact of Ionomers on AEMWE Performance.

Binders are of vital importance for AEMWEs.<sup>59</sup> As such, the impact of the prepared alkaline ionomers on AEMWE performance was investigated herein. The AEMWE cell was assembled with Yan's PAP-TP-85 as the AEM,<sup>60</sup> with the prepared alkaline ionomers used in the MEA with an iridium oxide (IrO<sub>2</sub>) anode (3.0 mg cm<sup>−2</sup>) and a platinum/carbon (Pt/C) cathode (1.5 mg cm<sup>−2</sup>), by the catalyst-coated substrate method. The corresponding mass loading of the alkaline ionomers in the CL was 0.75 mg cm<sup>−2</sup>. Figure 11 shows the polarization curves of the AEMWEs made with the alkaline ionomers working at 80 °C in a 1 M NaOH solution. The cell with the QP1-CF<sub>3</sub>-1, QP2-CF<sub>3</sub>-1, QP2-CF<sub>3</sub>-2, QP2-CF<sub>3</sub>-3, QP1-CN-1, QP2-CN-1, QP2-CN-2, and QP2-CN-3 ionomers displayed a current density of 1044, 1275, 1444, 1685, 780, 1107, 1276, and 1446 mA cm<sup>−2</sup> at 1.8 V, respectively. Despite similar IECs, the ionomers with spirobisindane monomers displayed a higher current density than those without the spirobisindane structure (QP2-CF<sub>3</sub>-1 vs QP1-CF<sub>3</sub>-1, QP2-CN-1 vs QP1-CN-1). Additionally, the CF<sub>3</sub>-substituted ionomers performed better than the CN-substituted series [QP1-CF<sub>3</sub>-1 vs QP1-CN-1, QP2-CF<sub>3</sub>-x vs QP2-CN-x (x = 1, 2, 3)]. Meanwhile, the in situ EIS was employed to measure the high-frequency resistance (HFR) of the cells. As shown in Figure S18, the HFR of these cells followed a similar order to the AEMWE performance of these alkaline ionomers. The utilization of the catalyst of the eight MEAs with these alkaline ionomers was analyzed based on hydrogen desorption according to the CV measurement, as shown in Figure S19a. The calculated ECSAs are summarized in Figure S19b. The CF<sub>3</sub>-substituted spirobisindane ionomers showed a higher ECSA than that of the CN-substituted series under similar IECs. In addition, the ECSA increases gradually as the proportion of spirobisindane units rises. A QP2-CF<sub>3</sub>-3-based MEA exhibits the highest ECSA of about 66.8 cm<sup>2</sup> mg<sub>Pt</sub><sup>−1</sup>, verifying the positive impact of the large free volumes on the activation of Pt catalyst sites in the CL. As all the MEAs were fabricated using the same procedure and AEM, the differential performance of the AEMWE was entirely dependent on the properties of the alkaline ionomers. We speculate that the main reason for the difference in performance is due to

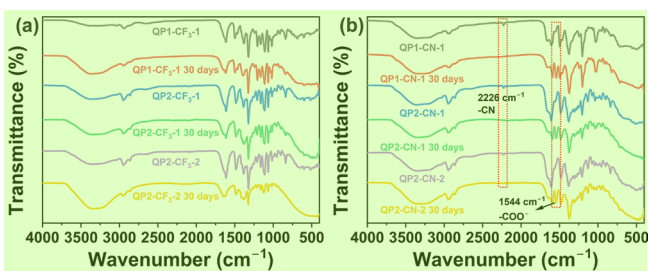
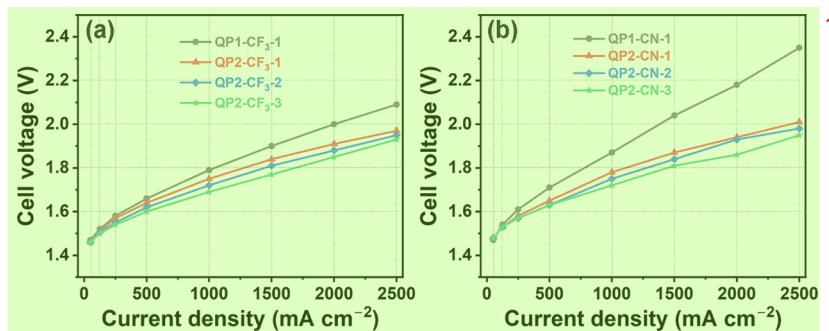


Figure 10. FTIR spectra changes of (a) QP1-CF<sub>3</sub>-1, QP2-CF<sub>3</sub>-1, and QP2-CF<sub>3</sub>-2 and (b) QP1-CN-1, QP2-CN-1, and QP2-CN-2 after immersion in a 1 M NaOH solution at 80 °C for 30 days.



**Figure 11.** Polarization curves measured during water electrolysis using (a) QP1-CF<sub>3</sub>-1 and QP2-CF<sub>3</sub>-1–3 and (b) QP1-CN-1 and QP2-CN-1–3 ionomers. Test conditions: the cell was operated at 80 °C in a 1 M NaOH solution using IrO<sub>2</sub> as the anode and Pt/C as the cathode.

**Table 3.** Comparison of the AEMWE Performances Obtained in this Study and Other Reported Studies

AEM	ionomer	cathode	anode	electrolyte	temperature (°C)	performance	ref.
PAP-TP-85	QP2-CF <sub>3</sub> -3	Pt/C	IrO <sub>2</sub>	1 M NaOH	80	1685 mA cm <sup>-2</sup> at 1.8 V	This work
PFOTFPPh-TMA-C8	PFOTFPPh-TMA-C8	Pt/C	IrO <sub>2</sub>	1 M KOH	80	1000 mA cm <sup>-2</sup> at 1.79 V	17
PQP-100	PBP-67	Pt/C	IrO <sub>2</sub>	1 M NaOH	85	1544 mA cm <sup>-2</sup> at 2.0 V	61
QBNTP	QAPBP	Pt/C	IrO <sub>2</sub>	1 M KOH	80	1900 mA cm <sup>-2</sup> at 2.0 V	62
FAA-3-50	PFPB-QA	Pt/C	IrO <sub>2</sub>	1 M KOH	70	946 mA cm <sup>-2</sup> at 2.0 V	63
HMT-PMBI	HMT-PMBI	Pt/C	Ir/C	1 M KOH	60	1000 mA cm <sup>-2</sup> at 1.74 V	64

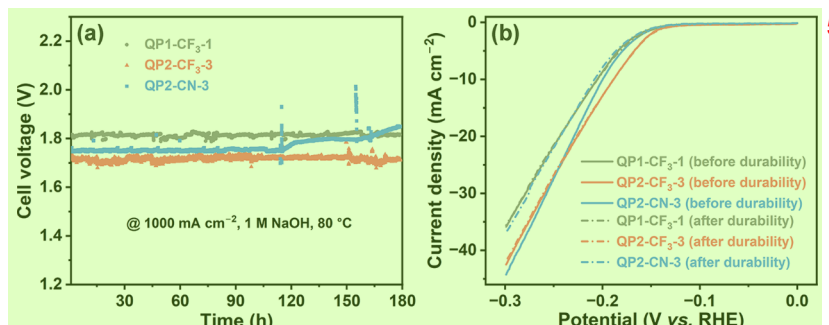


**Figure 12.** (a) Durability of the MEAs using the QP1-CF<sub>3</sub>-1, QP2-CF<sub>3</sub>-3, and QP2-CN-3 ionomers at a constant current density of 1000 mA cm<sup>-2</sup> fed with a 1 M NaOH solution at 80 °C. (b) LSV curves for QP1-CF<sub>3</sub>-1, QP2-CF<sub>3</sub>-3, and QP2-CN-3 before and after the durability test.

the increased microporosity of the CF<sub>3</sub>-substituted spirobisindane-containing ionomers. The larger free volumes endowed by the ionomer structures lead to improved transport of ions, water molecules, and gas products in the catalytic layer. These properties combine to give an overall improved performance in the AEMWEs. In addition, some AEMWE performances of other reported studies were provided for comparison in Table 3. The highly permeable alkaline ionomer showed excellent AEMWE performance, indicating that high gas permeability is very important for the development of high-performance ionomers.

The short-term durability of the MEAs using the QP1-CF<sub>3</sub>-1, QP2-CF<sub>3</sub>-3, and QP2-CN-3 ionomers was evaluated at a constant current density of 1000 mA cm<sup>-2</sup> fed with a 1 M NaOH solution at 80 °C. The durability profile is shown in Figure 12a. For the MEA using the QP2-CN-3 ionomer, irrecoverable performance loss was observed after 180 h of testing with the voltage increase from 1.75 to 1.85 V, even after refreshing the NaOH electrolyte. We speculate that the corresponding voltage increase is mainly due to the irreversible degradation of the QP2-CN-3 ionomer, leading to slower ion conduction. In contrast, the cell voltages of the MEAs using QP1-CF<sub>3</sub>-1 and QP2-CF<sub>3</sub>-3 remained almost constant during 180 h of operation despite at high current density, showing

significantly better durability than that of QP2-CN-3. Additionally, the LSV curves of water electrolysis cells before and after the durability test were also obtained to further prove the maintenance of the performance. As shown in Figure 12b, the MEAs using QP1-CF<sub>3</sub>-1 and QP2-CF<sub>3</sub>-3 as ionomers provided almost the same onset potential and current density before and after the durability test, indicating that there was no considerable activity lost during the durability test. In contrast, the LSV curve of the MEA using the QP2-CN-3 ionomer after the durability test displayed an evident difference, confirming that the irreversible degradation of the QP2-CN-3 ionomer induced the decreased electrocatalytic activity. In summary, these results demonstrate that the CF<sub>3</sub>-substituted ionomers own superior durability and are well suited to their use in MEAs.

#### 4. CONCLUSIONS

We have successfully designed two new monomers for ionomer synthesis: a single-benzene monomer (**1**) and a spirobisindane monomer (**2**). The monomers were used in varying ratios with 1,4-dimethoxybenzene and polymerized with two different aldehydes (*p*-trifluorobenzaldehyde and *p*-cyanobenzaldehyde) by methanesulfonic-acid-catalyzed Friedel–Crafts polycondensation. Subsequent quaternization of

the rigid triphenylmethane polymer precursors provided eight alkaline ionomers. It was found that the IEC values of the ionomers could be regulated by adjusting the proportion and structure of the monomers. The inherent microporosity, WU, SR, conductivity, microstructure, stability, and water electrolysis performance of these alkaline ionomers were systematically studied. Among these alkaline ionomers, QP2-CF<sub>3</sub>-3 displayed the highest surface area (69.0 m<sup>2</sup> g<sup>-1</sup>), OH<sup>-</sup> conductivity (144.4 mS cm<sup>-1</sup> @ 80 °C), alkaline stability (stable in 1 M NaOH @ 80 °C for 30 days), and current density (1685 mA cm<sup>-2</sup> at 1.8 V). Moreover, the MEA using the QP2-CF<sub>3</sub>-3 ionomer showed excellent durability at a high current density of 1000 mA cm<sup>-2</sup>. We hypothesize that its superior performance is due to its increased spirobisindane content and inert trifluoromethyl substitution. It has been demonstrated that these structural modifications lead to a higher free volume of the ionomer, promote the rapid conduction of ions and gas permeability, and enhance AEMWE performance. This study provides insights into structure–property relationships and presents a novel approach for the development of alkaline ionomers with high performance in AEMWEs.

## ASSOCIATED CONTENT

### Supporting Information

The Supporting Information is available free of charge at <https://pubs.acs.org/doi/10.1021/acs.macromol.3c00739>.

Synthesis procedure of 6,6'-dihydroxy-3,3,3',3'-tetra-methyl-1,1'-spirobisindane; <sup>1</sup>H NMR, <sup>13</sup>C NMR spectra, and HRMS of monomers; ionomer structure analysis (<sup>1</sup>H NMR spectra and FTIR spectra); and property characterization of the alkaline ionomers (viscosity, solubility, density, FFV, WU, SR, mechanical property, HFR, and ECSA) (PDF)

## AUTHOR INFORMATION

### Corresponding Authors

Boxin Xue – Shanghai Key Laboratory of Functional Materials Chemistry, Key Laboratory for Advanced Materials and School of Chemistry and Molecular Engineering, East China University of Science and Technology, Shanghai 200237, China; Ningbo Institute of Material Technology & Engineering, Chinese Academy of Sciences, Ningbo 315201, China; Email: [xueboxin@nimte.ac.cn](mailto:xueboxin@nimte.ac.cn)

Nanwen Li – State Key Laboratory of Coal Conversion, Institute of Coal Chemistry, Chinese Academy of Sciences, Taiyuan 030001, China; Center of Materials Science and Optoelectronics Engineering, University of Chinese Academy of Sciences, Beijing 100049, China; [orcid.org/0000-0002-2191-8123](https://orcid.org/0000-0002-2191-8123); Email: [linanwen@sxicc.ac.cn](mailto:linanwen@sxicc.ac.cn)

Pei-Nian Liu – Shanghai Key Laboratory of Functional Materials Chemistry, Key Laboratory for Advanced Materials and School of Chemistry and Molecular Engineering, East China University of Science and Technology, Shanghai 200237, China; [orcid.org/0000-0003-2014-2244](https://orcid.org/0000-0003-2014-2244); Email: [liupn@ecust.edu.cn](mailto:liupn@ecust.edu.cn)

### Authors

Shu-Qing Fu – Shanghai Key Laboratory of Functional Materials Chemistry, Key Laboratory for Advanced Materials and School of Chemistry and Molecular Engineering, East

China University of Science and Technology, Shanghai 200237, China

Bin Hu – State Key Laboratory of Coal Conversion, Institute of Coal Chemistry, Chinese Academy of Sciences, Taiyuan 030001, China; Center of Materials Science and Optoelectronics Engineering, University of Chinese Academy of Sciences, Beijing 100049, China

Ji-Hong Ge – Shanghai Key Laboratory of Functional Materials Chemistry, Key Laboratory for Advanced Materials and School of Chemistry and Molecular Engineering, East China University of Science and Technology, Shanghai 200237, China

Ming-Zhi Zhu – Shanghai Key Laboratory of Functional Materials Chemistry, Key Laboratory for Advanced Materials and School of Chemistry and Molecular Engineering, East China University of Science and Technology, Shanghai 200237, China

Pan-Pan Huang – Shanghai Key Laboratory of Functional Materials Chemistry, Key Laboratory for Advanced Materials and School of Chemistry and Molecular Engineering, East China University of Science and Technology, Shanghai 200237, China

Complete contact information is available at: <https://pubs.acs.org/10.1021/acs.macromol.3c00739>

### Author Contributions

<sup>1</sup>S.-Q.F. and B.H. contributed equally to this work.

### Notes

The authors declare no competing financial interest.

## ACKNOWLEDGMENTS

This work was supported by the National Natural Science Foundation of China (Nos. 21925201 and 22161160319), the Shanghai Sailing Program (21YF1409300), and the Fundamental Research Funds for the Central Universities. We thank the Research Center of Analysis and Test of East China University of Science and Technology for help in the characterization.

## REFERENCES

- (1) Xiao, L.; Zhang, S.; Pan, J.; Yang, C.; He, M.; Zhuang, L.; Lu, J. First Implementation of Alkaline Polymer Electrolyte Water Electrolysis Working Only with Pure Water. *Energy Environ. Sci.* **2012**, *5*, 7869–7871.
- (2) Park, E. J.; Capuano, C. B.; Ayers, K. E.; Bae, C. Chemically Durable Polymer Electrolytes for Solid-State Alkaline Water Electrolysis. *J. Power Sources* **2018**, *375*, 367–372.
- (3) Yang, Y.; Li, P.; Zheng, X.; Sun, W.; Dou, S. X.; Ma, T.; Pan, H. Anion-Exchange Membrane Water Electrolyzers and Fuel Cells. *Chem. Soc. Rev.* **2022**, *51*, 9620–9693.
- (4) Ehlers, J. C.; Feidenhans'l, A. A.; Therkildsen, K. T.; Larrazábal, G. O. Affordable Green Hydrogen from Alkaline Water Electrolysis: Key Research Needs from an Industrial Perspective. *ACS Energy Lett.* **2023**, *8*, 1502–1509.
- (5) Leng, Y.; Chen, G.; Mendoza, A. J.; Tighe, T. B.; Hickner, M. A.; Wang, C.-Y. Solid-State Water Electrolysis with an Alkaline Membrane. *J. Am. Chem. Soc.* **2012**, *134*, 9054–9057.
- (6) Li, D.; Park, E. J.; Zhu, W.; Shi, Q.; Zhou, Y.; Tian, H.; Lin, Y.; Serov, A.; Zulevi, B.; Baca, E. D.; Fujimoto, C.; Chung, H. T.; Kim, Y. S. Highly Quaternized Polystyrene Ionomers for High Performance Anion Exchange Membrane Water Electrolyzers. *Nat. Energy* **2020**, *5*, 378–385.

- (7) Hassan, N. U.; Zheng, Y.; Kohl, P. A.; Mustain, W. E. KOH vs Deionized Water Operation in Anion Exchange Membrane Electrolyzers. *J. Electrochem. Soc.* **2022**, *169*, No. 044526.
- (8) Li, Q.; Molina Villarino, A.; Peltier, C. R.; Macbeth, A. J.; Yang, Y.; Kim, M.-J.; Shi, Z.; Krumov, M. R.; Lei, C.; Rodríguez-Calero, G. G.; Soto, J.; Yu, S.-H.; Mutolo, P. F.; Xiao, L.; Zhuang, L.; Muller, D. A.; Coates, G. W.; Zelenay, P.; Abruna, H. D. Anion Exchange Membrane Water Electrolysis: The Future of Green Hydrogen. *J. Phys. Chem. C* **2023**, *127*, 7901–7912.
- (9) Wan, L.; Xu, Z.; Xu, Q.; Pang, M.; Lin, D.; Liu, J.; Wang, B. Key Components and Design Strategy of the Membrane Electrode Assembly for Alkaline Water Electrolysis. *Energy Environ. Sci.* **2023**, *16*, 1384–1430.
- (10) Li, D.; Motz, A. R.; Bae, C.; Fujimoto, C.; Yang, G.; Zhang, F.-Y.; Ayers, K. E.; Kim, Y. S. Durability of Anion Exchange Membrane Water Electrolyzers. *Energy Environ. Sci.* **2021**, *14*, 3393–3419.
- (11) Jang, M. J.; Yang, S. H.; Park, M. G.; Jeong, J.; Cha, M. S.; Shin, S.-H.; Lee, K. H.; Bai, Z.; Chen, Z.; Lee, J. Y.; Choi, S. M. Efficient and Durable Anion Exchange Membrane Water Electrolysis for a Commercially Available Electrolyzer Stack Using Alkaline Electrolyte. *ACS Energy Lett.* **2022**, *7*, 2576–2583.
- (12) Xu, Q.; Zhang, L.; Zhang, J.; Wang, J.; Hu, Y.; Jiang, H.; Li, C. Anion Exchange Membrane Water Electrolyzer: Electrode Design, Lab-Scaled Testing System and Performance Evaluation. *EnergyChem* **2022**, *4*, No. 100087.
- (13) Park, E. J.; Arges, C. G.; Xu, H.; Kim, Y. S. Membrane Strategies for Water Electrolysis. *ACS Energy Lett.* **2022**, *7*, 3447–3457.
- (14) Fan, J.; Willdorf-Cohen, S.; Schibli, E. M.; Paula, Z.; Li, W.; Skalski, T. J. G.; Sergeenko, A. T.; Hohenadel, A.; Friskin, B. J.; Magliocca, E.; Mustain, W. E.; Diesendruck, C. E.; Dekel, D. R.; Holdcroft, S. Poly(bis-arylimidazoliums) Possessing High Hydroxide Ion Exchange Capacity and High Alkaline Stability. *Nat. Commun.* **2019**, *10*, 2306.
- (15) Chu, X.; Shi, Y.; Liu, L.; Huang, Y.; Li, N. Piperidinium-Functionalized Anion Exchange Membranes and Their Application in Alkaline Fuel Cells and Water Electrolysis. *J. Mater. Chem. A* **2019**, *7*, 7717–7727.
- (16) Cha, M. S.; Park, J. E.; Kim, S.; Han, S.-H.; Shin, S.-H.; Yang, S. H.; Kim, T.-H.; Yu, D. M.; So, S.; Hong, Y. T.; Yoon, S. J.; Oh, S.-G.; Kang, S. Y.; Kim, O.-H.; Park, H. S.; Bae, B.; Sung, Y.-E.; Cho, Y.-H.; Lee, J. Y. Poly(carbazole)-Based Anion-Conducting Materials with High Performance and Durability for Energy Conversion Devices. *Energy Environ. Sci.* **2020**, *13*, 3633–3645.
- (17) Soni, R.; Miyanishi, S.; Kuroki, H.; Yamaguchi, T. Pure Water Solid Alkaline Water Electrolyzer Using Fully Aromatic and High-Molecular-Weight Poly(fluorene-alt-tetrafluorophenylene)-Trimethyl Ammonium Anion Exchange Membranes and Ionomers. *ACS Appl. Energy Mater.* **2020**, *4*, 1053–1058.
- (18) Lindquist, G. A.; Oener, S. Z.; Krivina, R.; Motz, A. R.; Keane, A.; Capuano, C.; Ayers, K. E.; Boettcher, S. W. Performance and Durability of Pure-Water-Fed Anion Exchange Membrane Electrolyzers Using Baseline Materials and Operation. *ACS Appl. Mater. Interfaces* **2021**, *13*, 51917–51924.
- (19) Wang, X.; Qiao, X.; Liu, S.; Liu, L.; Li, N. Poly(terphenyl piperidinium) Containing Hydrophilic Crown Ether Units in Main Chains as Anion Exchange Membranes for Alkaline Fuel Cells and Water Electrolyzers. *J. Membr. Sci.* **2022**, *653*, No. 120558.
- (20) Suo, X.; Yu, Y.; Qian, S.; Zhou, L.; Cui, X.; Xing, H. Tailoring the Pore Size and Chemistry of Ionic Ultramicroporous Polymers for Trace Sulfur Dioxide Capture with High Capacity and Selectivity. *Angew. Chem., Int. Ed.* **2021**, *60*, 6986–6991.
- (21) Chen, X.; Fan, Y.; Wu, L.; Zhang, L.; Guan, D.; Ma, C.; Li, N. Ultra-Selective Molecular-Sieving Gas Separation Membranes Enabled by Multi-Covalent-Crosslinking of Microporous Polymer Blends. *Nat. Commun.* **2021**, *12*, 6140.
- (22) Lai, H. W. H.; Benedetti, F. M.; Ahn, J. M.; Robinson, A. M.; Wang, Y.; Pinnau, I.; Smith, Z. P.; Xia, Y. Hydrocarbon Ladder Polymers with Ultrahigh Permselectivity for Membrane Gas Separations. *Science* **2022**, *375*, 1390–1392.
- (23) Hu, C.; Zhang, Q.; Lin, C.; Lin, Z.; Li, L.; Soyeckwo, F.; Zhu, A.; Liu, Q. Multi-Cation Crosslinked Anion Exchange Membranes from Microporous Tröger's Base Copolymers. *J. Mater. Chem. A* **2018**, *6*, 13302–13311.
- (24) Zuo, P.; Li, Y.; Wang, A.; Tan, R.; Liu, Y.; Liang, X.; Sheng, F.; Tang, G.; Ge, L.; Wu, L.; Song, Q.; McKeown, N. B.; Yang, Z.; Xu, T. Sulfonated Microporous Polymer Membranes with Fast and Selective Ion Transport for Electrochemical Energy Conversion and Storage. *Angew. Chem., Int. Ed.* **2020**, *59*, 9564–9573.
- (25) Wang, X.; Guo, H.; Yu, C.; Jing, Y.; Han, Z.; Ma, X.; Yang, C.; Liu, M.; Zhai, D.; Zheng, D.; Pan, Y.; Li, X.; Ding, K. Practical Enantioselective Synthesis of Chiroptical Polymers of Intrinsic Microporosity with Circular Polarized Luminescence. *Macromolecules* **2021**, *54*, 11180–11186.
- (26) Yang, Z.; Guo, R.; Malpass-Evans, R.; Carta, M.; McKeown, N. B.; Guiver, M. D.; Wu, L.; Xu, T. Highly Conductive Anion-Exchange Membranes from Microporous Tröger's Base Polymers. *Angew. Chem., Int. Ed.* **2016**, *55*, 11499–11502.
- (27) Li, Z.; Guo, J.; Zheng, J.; Sherazi, T. A.; Li, S.; Zhang, S. A Microporous Polymer with Suspended Cations for Anion Exchange Membrane Fuel Cells. *Macromolecules* **2020**, *53*, 10998–11008.
- (28) Wang, Q.; Huang, L.; Wang, Z.; Zheng, J.; Zhang, Q.; Qin, G.; Li, S.; Zhang, S. High Conductive Anion Exchange Membranes from All-Carbon Twisted Intrinsic Microporous Polymers. *Macromolecules* **2022**, *55*, 10713–10722.
- (29) Chen, W.-F.; Lin, H.-Y.; Dai, S. A. Generation and Synthetic Uses of Stable 4-[2-Isopropylidene]-Phenol Carbocation from Bisphenol A. *Org. Lett.* **2004**, *6*, 2341–2343.
- (30) Wang, X.; Cui, M.; Yu, P.; Li, Z.; Yang, Y.; Jia, H.; Liu, B. Synthesis and Biological Evaluation of Novel Technetium-99m Labeled Phenylbenzoxazole Derivatives as Potential Imaging Probes for  $\beta$ -Amyloid Plaques in Brain. *Bioorg. Med. Chem. Lett.* **2012**, *22*, 4327–4331.
- (31) Zhang, Z.; Wu, L.; Varcoe, J.; Li, C.; Ong, A. L.; Poynton, S.; Xu, T. Aromatic Polyelectrolytes Via Polyacylation of Pre-Quaternized Monomers for Alkaline Fuel Cells. *J. Mater. Chem. A* **2013**, *1*, 2595–2601.
- (32) Zhu, H.; Sun, Z.; Cao, H.; Wang, B.; Zhao, J.; Pan, J.; Xu, G.; Jin, Z.; Yan, F. Highly Conductive and Dimensionally Stable Anion Exchange Membranes Based on Poly(dimethoxybenzene-co-methyl 4-formylbenzoate) Ionomers. *Macromolecules* **2021**, *54*, 5557–5566.
- (33) Zou, L.; Cao, X.; Zhang, Q.; Dodds, M.; Guo, R.; Gao, H. Friedel–Crafts  $A_2 + B_4$  Polycondensation toward Regioselective Linear Polymer with Rigid Triphenylmethane Backbone and Its Property as Gas Separation Membrane. *Macromolecules* **2018**, *51*, 6580–6586.
- (34) Zhou, S.; Guan, J.; Li, Z.; Zhang, Q.; Zheng, J.; Li, S.; Zhang, S. Synthesis of Fluorinated Poly(phenyl-alkane)s of Intrinsic Microporosity by Regioselective Aldehyde ( $A_2$ ) + Aromatics ( $B_2$ ) Friedel–Crafts Polycondensation. *Macromolecules* **2021**, *54*, 6543–6551.
- (35) Xue, B.; Zhu, M.-Z.; Fu, S.-Q.; Huang, P.-P.; Qian, H.; Liu, P.-N. Facile Synthesis of Sulfonated Poly(phenyl-alkane)s for Proton Exchange Membrane Fuel Cells. *J. Membr. Sci.* **2023**, *673*, No. 121263.
- (36) Zhou, S.; Lin, X.; Hu, Y.; Fu, L.; Luo, Q.; Yang, L.; Hou, S.; Kong, X.-Y.; Jiang, L.; Wen, L. Tailoring Sulfonated Poly(phenyl-alkane)s of Intrinsic Microporosity Membrane for Advanced Osmotic Energy Conversion. *ACS Mater. Lett.* **2022**, *4*, 1422–1429.
- (37) Guzmán-Gutiérrez, M. T.; Nieto, D. R.; Fomine, S.; Morales, S. L.; Zolotukhin, M. G.; Hernandez, M. C. G.; Kricheldorf, H.; Wilks, E. S. Dramatic Enhancement of Superacid-Catalyzed Polyhydroxyalkylation Reactions. *Macromolecules* **2011**, *44*, 194–202.
- (38) Cruz, A. R.; Hernandez, M. C. G.; Guzmán-Gutiérrez, M. T.; Zolotukhin, M. G.; Fomine, S.; Morales, S. L.; Kricheldorf, H.; Wilks, E. S.; Cárdenas, J.; Salmón, M. Precision Synthesis of Narrow Polydispersity, Ultrahigh Molecular Weight Linear Aromatic Poly-

- mers by A<sub>2</sub> + B<sub>2</sub> Nonstoichiometric Step-Selective Polymerization. *Macromolecules* **2012**, *45*, 6774–6780.
- (39) He, Q.; Xu, T.; Qian, H.; Zheng, J.; Shi, C.; Li, Y.; Zhang, S. Enhanced Proton Conductivity of Sulfonated Poly(*p*-phenylene-*co*-aryl ether ketone) Proton Exchange Membranes with Controlled Microblock Structure. *J. Power Sources* **2015**, *278*, 590–598.
- (40) Allushi, A.; Bakvand, P. M.; Jannasch, P. Polyfluorenes Bearing N,N-Dimethylpiperidinium Cations on Short Spacers for Durable Anion Exchange Membranes. *Macromolecules* **2023**, *56*, 1165–1176.
- (41) Li, L.; Jiang, T.; Wang, S.; Cheng, S.; Li, X.; Wei, H.; Ding, Y. Branched Anion-Conducting Poly(arylene alkylene)s for Alkaline Membrane Fuel Cells. *ACS Appl. Energy Mater.* **2022**, *5*, 2462–2473.
- (42) Yang, Y.; Jiang, T.; Li, L.; Zhou, S.; Fang, H.; Li, X.; Wei, H.; Ding, Y. Chemo-Stable Poly(quinquephenylene-*co*-diphenylene piperidinium) Ionomers for Anion Exchange Membrane Fuel Cells. *J. Power Sources* **2021**, *506*, No. 230184.
- (43) Jiang, T.; Wang, C.; Wang, T.; Wang, X.; Wang, X.; Li, X.; Ding, Y.; Wei, H. Imidazolium Structural Isomer Pyrazolium: A Better Alkali-Stable Anion Conductor for Anion Exchange Membranes. *J. Membr. Sci.* **2022**, *660*, No. 120843.
- (44) Liu, B.; Li, T.; Li, Q.; Zhu, S.; Duan, Y.; Li, J.; Zhang, H.; Zhao, C. Enhanced Diffusion Dialysis Performance of Cross-Linked Poly(aryl piperidine) Anion Exchange Membranes by Thiol-Ene Click Chemistry for Acid Recovery. *J. Membr. Sci.* **2022**, *660*, No. 120816.
- (45) Hou, J.; Liu, Y.; Liu, Y.; Wu, L.; Yang, Z.; Xu, T. Self-Healing Anion Exchange Membrane for pH 7 Redox Flow Batteries. *Chem. Eng. Sci.* **2019**, *201*, 167–174.
- (46) Li, L.; Zhang, J.; Jiang, T.; Sun, X.; Li, Y.; Li, X.; Yang, S.; Lu, S.; Wei, H.; Ding, Y. High Ion Conductivity and Diffusivity in the Anion Exchange Membrane Enabled by Tethering with Multication Strings on the Poly(biphenyl alkylene) Backbone. *ACS Appl. Energy Mater.* **2020**, *3*, 6268–6279.
- (47) Wang, T.; Zhao, Y.; Ma, R.; Li, L.; Ling, Q.; Li, X.; Ding, Y.; Wei, H. Highly Conductive and Dimensionally Stable Anion Exchange Membranes Enabled by Rigid Poly(arylene alkylene) Backbones. *Synth. Met.* **2023**, *296*, No. 117385.
- (48) Xie, Y.; Li, S.; Pang, J.; Jiang, Z. Micro-Block Poly(arylene ether sulfone)s with Densely Quaternized Units for Anion Exchange Membranes: Effects of Benzyl N-Methylpiperidinium and Benzyl Trimethyl Ammonium Cations. *J. Membr. Sci.* **2023**, *669*, No. 121333.
- (49) Xue, B.; Cui, W.; Zhou, S.; Zhang, Q.; Zheng, J.; Li, S.; Zhang, S. Facile Preparation of Highly Alkaline Stable Poly(arylene-imidazolium) Anion Exchange Membranes through an Ionized Monomer Strategy. *Macromolecules* **2021**, *54*, 2202–2212.
- (50) Xiao, Y.; Xu, J.; Hu, L.; Wang, H.; Gao, L.; Peng, S.; Di, M.; Sun, X.; Liu, J.; Yan, X.; Chen, L.; He, G. Advanced Anion-Selective Membranes with Pendant Quaternary Ammonium for Neutral Aqueous Supporting Redox Flow Battery. *J. Membr. Sci.* **2022**, *659*, No. 120748.
- (51) Dong, Z.; Di, M.; Hu, L.; Gao, L.; Yan, X.; Ruan, X.; Wu, X.; He, G. Hydrophilic/Hydrophobic-*bi*-Comb-Shaped Amphoteric Membrane for Vanadium Redox Flow Battery. *J. Membr. Sci.* **2020**, *608*, No. 118179.
- (52) Wang, C.; Tao, Z.; Zhou, Y.; Zhao, X.; Li, J.; Ren, Q.; Guiver, M. D. Anion Exchange Membranes with Eight Flexible Side-Chain Cations for Improved Conductivity and Alkaline Stability. *Sci. China Mater.* **2020**, *63*, 2539–2550.
- (53) Gou, W. W.; Gao, W. T.; Gao, X. L.; Zhang, Q. G.; Zhu, A. M.; Liu, Q. L. Highly Conductive Fluorinated Poly(biphenyl piperidinium) Anion Exchange Membranes with Robust Durability. *J. Membr. Sci.* **2022**, *645*, No. 120200.
- (54) Liu, F.; Miyatake, K. Well-Designed Polyphenylene PEMs with High Proton Conductivity and Chemical and Mechanical Durability for Fuel Cells. *J. Mater. Chem. A* **2022**, *10*, 7660–7667.
- (55) Chu, F.; Chu, X.; Zhang, S.; Zhu, H.; Ren, Y.; Han, J.; Xie, R.; Lin, B.; Ding, J. Cross-Linked Spirocyclic Quaternary Ammonium-Based Anion Exchange Membrane with Tunable Properties for Fuel Cell Applications. *ChemistrySelect* **2019**, *4*, 5269–5275.
- (56) Zhang, Y.; Chen, W.; Yan, X.; Zhang, F.; Wang, X.; Wu, X.; Pang, B.; Wang, J.; He, G. Ether Spaced N-Spirocyclic Quaternary Ammonium Functionalized Crosslinked Polysulfone for High Alkaline Stable Anion Exchange Membranes. *J. Membr. Sci.* **2020**, *598*, No. 117650.
- (57) Jeon, J. W.; Kim, D.-G.; Sohn, E.-H.; Yoo, Y.; Kim, Y. S.; Kim, B. G.; Lee, J.-C. Highly Carboxylate-Functionalized Polymers of Intrinsic Microporosity for CO<sub>2</sub>-Selective Polymer Membranes. *Macromolecules* **2017**, *50*, 8019–8027.
- (58) Dong, X.; Xue, B.; Qian, H.; Zheng, J.; Li, S.; Zhang, S. Novel Quaternary Ammonium Microblock Poly(*p*-phenylene-*co*-aryl ether ketone)s as Anion Exchange Membranes for Alkaline Fuel Cells. *J. Power Sources* **2017**, *342*, 605–615.
- (59) Chen, N.; Paek, S. Y.; Lee, J. Y.; Park, J. H.; Lee, S. Y.; Lee, Y. M. High-Performance Anion Exchange Membrane Water Electrolyzers with a Current Density of 7.68 A cm<sup>-2</sup> and a Durability of 1000 Hours. *Energy Environ. Sci.* **2021**, *14*, 6338–6348.
- (60) Wang, J.; Zhao, Y.; Setzler, B. P.; Rojas-Carbonell, S.; Ben Yehuda, C.; Amel, A.; Page, M.; Wang, L.; Hu, K.; Shi, L.; Gottesfeld, S.; Xu, B.; Yan, Y. Poly(aryl piperidinium) Membranes and Ionomers for Hydroxide Exchange Membrane Fuel Cells. *Nat. Energy* **2019**, *4*, 392–398.
- (61) Liu, M.; Hu, X.; Hu, B.; Liu, L.; Li, N. Soluble Poly(aryl piperidinium) with Extended Aromatic Segments as Anion Exchange Membranes for Alkaline Fuel Cells and Water Electrolysis. *J. Membr. Sci.* **2022**, *642*, No. 119966.
- (62) Gao, W. T.; Gao, X. L.; Choo, Y. S. L.; Wang, J. J.; Cai, Z. H.; Zhang, Q. G.; Zhu, A. M.; Liu, Q. L. Durable Dual-Methylpiperidinium Crosslinked Poly(binaphthyl-*co*-terphenyl piperidinium) Anion Exchange Membranes with High Ion Transport and Electrochemical Performance. *Chem. Eng. J.* **2023**, *466*, No. 143107.
- (63) Lim, H.; Jeong, I.; Choi, J.; Shin, G.; Kim, J.; Kim, T.-H.; Park, T. Anion Exchange Membranes and Ionomer Properties of a Polyfluorene-Based Polymer with Alkyl Spacers for Water Electrolysis. *Appl. Surf. Sci.* **2023**, *610*, No. 155601.
- (64) Chen, B.; Mardle, P.; Holdcroft, S. Probing the Effect of Ionomer Swelling on the Stability of Anion Exchange Membrane Water Electrolyzers. *J. Power Sources* **2022**, *550*, No. 232134.